

# Electronic phases of low dimensional conductors

C. Bourbonnais

Centre de Recherche sur les Propriétés Électroniques de Matériaux Avancées,  
Département de Physique Université de Sherbrooke, Sherbrooke, Québec, Canada  
J1K 2R1

**Abstract.** We briefly review the physics of electronic phases in low dimensional conductors. We begin by introducing the properties of the one-dimensional electron gas model using bosonization and renormalization group methods. We then tackle the influence of interchain coupling and go through the different instabilities of the electron system to the formation of higher dimensional states. The connection with observations made in quasi-one-dimensional organic and inorganic conductors is discussed.

## 1 Introduction

There is a *consensus generalis* about the impact of reducing spatial dimension in systems of interacting electrons: correlation effects are magnified and range of electronic behaviors expanded. This is well exemplified in one spatial dimension where low energy electronic excitations turn out to be entirely collective in character so that a description in terms of Fermi liquid quasi-particles, which proved to be so successful in isotropic systems, becomes simply inapplicable.

Organic conductors belong to a class of crystals for which the planar conformation of the molecular constituents combined with their packing as weakly coupled chains in the solid state yield close realizations of one-dimensional solids. Quasi-one dimensional electronic structures are also found in inorganic materials such as the molybdenum bronzes, the chalcogenides and ladder cuprates,<sup>1</sup> as a result of their peculiar molecular or atomic arrangements. In all these quasi-one-dimensional crystals, we are thus faced with a twofold difficulty which combines the objective of determining the temperature range where one-dimensional physics applies with the one of finding the origin of low temperature higher dimensional states. In this review, we will be mainly concerned with these two closely bound issues that are at the heart of the description of the rich phase diagram of compounds like the Bechgaard salt series  $((TMTSF)_2X)$  and their sulfur analogs, the Fabre salt series  $((TMTTF)_2X)$ , where  $X = PF_6, AsF_6 \dots$  is a monovalent anion).

In the first part of this review, we shall briefly outline the non Fermi liquid properties of the one-dimensional electron gas using bosonization and renormalization group methods. We then consider the problem of instabilities of one-dimensional electronic states by introducing the coupling between chains. We

<sup>1</sup> See the reviews of D. Jérôme and T. M. Rice on ladder systems in this volume. Luttinger liquid behavior from edge states of two-dimensional electron gas in quantum well structures is discussed by C. Glattli in this volume.

discuss subsequently how the concepts of low-dimensional physics prove relevant when one tries to construct a coherent picture of electronic states that are actually found in quasi-one-dimensional organic compounds. We close this review with a brief discussion on the importance of one-dimensional physics in inorganic metals like the molybdenum bronzes.

## 2 Interacting electrons in one dimension

### 2.1 The Tomanaga-Luttinger model

When one tries to understand the origin of non-Fermi-liquid behavior in one dimension,<sup>2</sup> it is instructive to look first at the possible elementary excitations such a low dimensional system can sustain. Consider the transfer of an electron in the final state of wave vector  $k + q$  above a filled Fermi sea. Together with the hole left at  $k$ , both particles form an electron-hole elementary excitation of energy  $\omega(q) = \epsilon(k + q) - \epsilon(k)$  ( $\hbar = 1$ ). In one dimension, the available phase space below  $\omega(q)$  for the decay of such excitations shrinks to zero at low energy, namely where the spectrum

$$\epsilon(k) \rightarrow \epsilon_p(k) = v_F(pk - k_F) \quad (1)$$

can be considered as *linear*. A linear spectrum with an unbounded interval of  $k$  values for each branch  $p = \pm$  (referring to right (+) and left (−) moving electrons) defines the spectrum of the Luttinger model.[4] In these conditions, electron-hole excitations acquire a high degree of degeneracy  $\sim qL/2\pi$ . It follows that stable charge and spin-density excitations can be formed from the superpositions of excitations

$$\rho_{\pm}(q) = \frac{1}{\sqrt{2}} \sum_{\alpha, k} a_{\pm, k+q, \alpha}^{\dagger} a_{\pm, k, \alpha} \quad (2)$$

for the charge and

$$\sigma_{\pm}(q) = \frac{1}{\sqrt{2}} \sum_{\alpha, k} \alpha a_{\pm, k+q, \alpha}^{\dagger} a_{\pm, k, \alpha} \quad (3)$$

for the spin. This connotes that a free – bosonic – Hamiltonian may exist for the description of collective charge and spin modes. Actually for a Luttinger spectrum with all negative energy states filled, [5] these composite objects obey the commutation rules

$$[\rho_p(q), \rho_{p'}(-q)] = p\delta_{pp'} q \frac{L}{2\pi}$$

---

<sup>2</sup> We refer to the excellent reviews of J. Voit [1], H. J. Schulz [2] and V. J. Emery [3] for a more exhaustive discussion of the one-dimensional gas model using bosonization method.

$$[\sigma_p(q), \sigma_{p'}(-q)] = p\delta_{pp'} q \frac{L}{2\pi}, \quad (4)$$

which are compatible with bosons. Another key feature is the commutation relation between the one-electron Hamiltonian

$$H_0 = \sum_{k,p,\alpha} \epsilon_p(k) a_{p,k,\alpha}^\dagger a_{p,k,\alpha} \quad (5)$$

and the spin and charge-density operators:

$$\begin{aligned} [H_0, \rho_p(q)] &= p v_F q \rho_p(q) \\ [H_0, \sigma_p(q)] &= p v_F q \sigma_p(q), \end{aligned} \quad (6)$$

which reminds the algebra of operators for the harmonic oscillator. A fermion to boson correspondance for the excitations can thus be established in which  $H_0$  can be written as

$$H_0 = \sum_{p,q} p v_F q (\bar{\rho}_p(q) \bar{\rho}_p(-q) + \bar{\sigma}_p(q) \bar{\sigma}_p(-q)), \quad (7)$$

which is quadratic in the charge  $\bar{\rho}_p \equiv (2\pi/Lq)^{\frac{1}{2}} \rho_p$  and spin  $\bar{\sigma}_p \equiv (2\pi/Lq)^{\frac{1}{2}} \sigma_p$  operators. All the excited states of the fermion system can then be described in terms of bosonic variables.

In the Tomanaga-Luttinger model,[6,4] electrons interact through the exchange of small momentum transfer. This allows us to define two scattering processes usually denoted  $g_2$  and  $g_4$  couplings with respect to the Fermi points  $\pm k_F$  (here taken for simplicity as  $q$ -independent interactions [5,7]). The total Hamiltonian becomes  $H_{TL} = H_0 + H_I$ , in which the interacting part  $H_I$  can also be expressed in terms of density operators:

$$\begin{aligned} H_I &= \frac{1}{L} \sum_{\alpha_1,2} \sum_{k_1,k_2,q} g_2 a_{+,k_1+q,\alpha_1}^\dagger a_{-,k_2-q,\alpha_2}^\dagger a_{-k_2,\alpha_2} a_{+,k_1,\alpha_1} \\ &\quad + \frac{1}{L} \sum_{\alpha,p} \sum_{k_1,k_2,q} g_4 a_{p,k_1+q,\alpha}^\dagger a_{p,k_2-q,-\alpha}^\dagger a_{pk_2,-\alpha} a_{p,k_1,\alpha} \\ &= 2g_2 \sum_{p,q} v_F q \bar{\rho}_p(q) \bar{\rho}_{-p}(-q) + g_4 \sum_{p,q} v_F q (\bar{\rho}_p(q) \bar{\rho}_p(-q) - \bar{\sigma}_p(q) \bar{\sigma}_p(-q)). \end{aligned} \quad (8)$$

The TL Hamiltonian is therefore still quadratic in terms of the bosonic operators. Owing to the presence of the  $g_2$  term which couples the density on different branches, a transformation is needed to diagonalize the Hamiltonian. We thus have

$$\begin{aligned} H_{TL} &= H_\sigma + H_\rho \\ &= \sum_{p,q} \omega_\sigma(q) b_{\sigma,q}^\dagger b_{\sigma,q} + \omega_\rho(q) b_{\rho,q}^\dagger b_{\rho,q}, \end{aligned} \quad (9)$$

in which the new operators  $b_\sigma^{(\dagger)}$  for spin and  $b_\rho^{(\dagger)}$  for charge obey boson commutation rules. The spin and charge spectra of collective excitations have a Debye

form  $\omega_\nu(q) = u_\nu | q |$  ( $\nu = \sigma, \rho$ ), where the velocities are

$$u_\sigma = v_F \left( 1 - \frac{g_4}{2\pi v_F} \right) \quad (10)$$

for the spin and

$$u_\rho = v_\rho \left( 1 - \left( \frac{g_2}{\pi v_\rho} \right)^2 \right)^{1/2} \quad (11)$$

for the charge, with  $v_\rho = v_F(1 + g_4/2\pi v_F)$ . A key property of the above Hamiltonian is the commutation relation  $[H_\sigma, H_\rho] = 0$ , which yields the decoupling between  $H_\sigma$  and  $H_\rho$  that is termed *separation between spin and charge degrees of freedom*. The corresponding split-off of acoustic excitations will have a profound influence on the properties of the system which becomes a Luttinger liquid.[8] As regards thermodynamics, the free energy will consist of two separate contributions, which yields the property of additivity for the specific heat (per unit of length)  $C = C_\sigma + C_\rho$ . Here  $C_{\nu=\sigma,\rho} = \pi k_B^2 T / (3u_\nu)$  is the linear temperature dependent specific heat of each branch of acoustic excitations.

## 2.2 Phase variables description

Collective excitations in a Luttinger liquid are reminiscent of those of a vibrating string. This relation can be further sharpened if one introduces the pair of conjugate phase variables

$$\begin{aligned} \phi_\nu(x) &= -i \frac{\pi}{L} \sum_q \frac{e^{-iqx}}{q} e^{-\alpha_0|q|/2} [\nu_+(q) + \nu_-(q)] \\ \Pi_\nu(x) &= i \frac{1}{L} \sum_q e^{-iqx} e^{-\alpha_0|q|/2} [\nu_+(q) - \nu_-(q)], \end{aligned} \quad (12)$$

which satisfy commutation relation  $[\phi_\nu(x_1), \Pi_{\nu'}(x_2)] = i\delta_{\nu,\nu'}\delta(x_1 - x_2)$  in the limit  $\alpha_0 \rightarrow 0$  for the short distance cut-off.

The phase variable representation allows us to rewrite the Tomonaga-Luttinger Hamiltonian in the harmonic form

$$H_{TL} = \sum_{\nu=\rho,\sigma} \frac{1}{2} \int \left[ \pi u_\nu K_\nu \Pi_\nu^2 + u_\nu (\pi K_\nu)^{-1} \left( \frac{\partial \phi_\nu}{\partial x} \right)^2 \right] dx, \quad (13)$$

where  $K_\nu$  is the stiffness constants of acoustic excitations. The properties of the model are then entirely governed by the set of parameters  $\{u_\nu, K_\nu\}$ . These are functions of the microscopic coupling constants. Thus for a rotationally invariant system (spin independent interactions), one has  $K_\sigma = 1$  and

$$K_\rho = \left( \frac{2\pi v_F + g_4 - 2g_2}{2\pi v_F + g_4 + 2g_2} \right)^{1/2}. \quad (14)$$

### 2.3 Properties of the Luttinger liquid state

**One-particle** Consider the Matsubara time-ordered single-particle Green's function  $G_p(x, \tau) = -\langle T_\tau \psi_{p,\alpha}(x, \tau) \psi_{p,\alpha}^\dagger(0, 0) \rangle$ , which is expressed as a statistical average over fermion fields. It can be evaluated explicitly by using the harmonic phase Hamiltonian (13), with the aid of the relation between the Fermi and bosonic fields [9,10,11]:

$$\begin{aligned} \psi_{p,\alpha}(x) &= L^{-\frac{1}{2}} \sum_k a_{p,k,\alpha} e^{ikx} \\ &\sim \lim_{\alpha_0 \rightarrow 0} \frac{e^{ipk_F x}}{\sqrt{2\pi\alpha_0}} \exp\left(-\frac{i}{\sqrt{2}}[p(\phi_\rho + \alpha\phi_\sigma) + (\theta_\rho + \alpha\theta_\sigma)]\right), \end{aligned} \quad (15)$$

where  $\theta_\nu(x) = \pi \int \Pi_\nu(x') dx'$ . One finds

$$G_p(x, \tau) = \frac{e^{ipk_F x}}{\alpha_0^{-\theta}} \prod_\nu [\xi_\nu \sinh(x + iu_\nu \tau)/\xi_\nu]^{-\frac{1}{2} - \theta_\nu} [\xi_\nu \sinh(x - iu_\nu \tau)/\xi_\nu]^{-\theta_\nu} \quad (16)$$

where  $\theta_\nu = \frac{1}{4}(K_\nu + 1/K_\nu - 2)$ . As a correlation function of the electron with itself, the Green's function gives useful information about the spatial and time decay of single-particle quantum coherence in the presence of collective oscillations of the Luttinger liquid. At equal Matsubara time, which amounts to put  $\tau = 0$  in the above expression, we observe that  $G_p$  depends on two characteristic length scales  $\xi_\sigma = u_\sigma/\pi T$  and  $\xi_\rho = u_\rho/\pi T$ , corresponding to the de Broglie quantum lengths for spin and charge acoustic excitations. Thus for  $\alpha_0 \ll x \ll \xi_\nu$ , the fermion coherence decays according to the power law

$$G_p(x) \approx \frac{e^{ipk_F x}}{\alpha_0^{-\theta}} \frac{1}{x^{1+\theta}}, \quad (17)$$

where the exponent  $\theta = \theta_\sigma + \theta_\rho$  is called the anomalous dimension of the Green's function. It is non-zero in the presence of interaction (the canonical dimension of the Green's function is unity in a free electron gas). For non-zero interaction, the spatial decay of quasi-particle coherence is therefore faster. The existence of a anomalous power law is also the mark of scaling (a situation analogous to one of correlations of the order parameter at the critical point), namely the absence of particular length scale of the fermion coherence between  $\alpha_0$  and  $\xi_\nu$ .

For large distances  $x \gg \xi_\nu$ , we have

$$G_p(x) \propto e^{-x/\xi}, \quad (18)$$

indicating that thermal fluctuations lead to an exponential decay of coherence and the absence of scaling. The effective coherence length  $\xi^{-1} = 1/\xi_\sigma + 1/\xi_\rho$  combines the spin and the charge quantum lengths.

The absence of ordinary quasi-particle states in a Luttinger liquid will also show up in the one-electron spectral properties. These can be extracted from the

Fourier transform of the retarded Green's function. The quantity of interest is the spectral weight defined as the imaginary part of the Green's function:

$$A_p(q, \omega) = -\frac{1}{\pi} \text{Im}G_p(pk_F + q, \omega), \quad (19)$$

which gives the probability of having a single-particle state of wave vector  $pk_F + q$  with a energy  $\omega$  measured from the Fermi level. The spectral function takes on particular importance since it can be probed at  $q < 0$  ( $q > 0$ ) by photoemission (inverse photoemission) experiments. We will focus here on spin independent interactions for which  $K_\sigma = 1$  and  $\theta_\sigma = 0$ . The presence of collective modes with two different velocities in a Luttinger liquid has a pronounced influence on the spectral function in comparison to that of a Fermi liquid. In the latter case, the spectral weight  $A_p(\omega) = z\delta(\omega)$  is simply a delta function at the Fermi edge indicating the presence of well defined quasi-particle excitations of weight  $z$  at zero temperature. At finite temperature or finite  $q$ , there is the usual broadening of the quasi-particle peak ( $\sim T^2$  or  $v_F^2 q^2$ ).

The progress made to achieve the Fourier transform of  $G_p(x, \tau \rightarrow it)$  at zero temperature,[12,13] indicates instead the absence of quasi-particle peak in the spectral weight. In effect, collective modes suppresses the delta function, which is replaced at not too large  $\theta$  by power law singularities

$$\begin{aligned} A_+(k_F + q, \omega) &\sim_{\omega \rightarrow u_\rho q} |\omega - u_\rho q|^{\frac{1}{2}\theta - \frac{1}{2}} \\ &\sim_{\omega \rightarrow u_\sigma q} \Theta(\omega - u_\sigma q)(\omega - u_\sigma q)^{\theta - \frac{1}{2}} \\ &\sim_{\omega \rightarrow -u_\sigma q} \Theta(-\omega - u_\rho q)(-\omega - u_\rho q)^{\frac{1}{2}\theta}, \end{aligned} \quad (20)$$

for  $q > 0$ .[12] At finite temperature,[14,15] thermal broadening will round singularities and cusps.

Another physical quantity of interest is the one-electron density of states (per spin)

$$\begin{aligned} N(\omega) &= \sum_p \int \frac{dq}{2\pi} A_p(q, \omega) \\ &\propto |\omega|^\theta. \end{aligned} \quad (21)$$

In a Luttinger liquid, the density of states is not constant but presents a dip close to the Fermi level.[16] Strickly at the Fermi level, the density of states is zero showing once again the absence of quasi-particles at  $T = 0$ . At finite temperature,  $N(T) \propto T^\theta$ , the dip partly fills at the Fermi level due to thermal fluctuations.

**Two-particle response** The two-particle response function in Matsubara-Fourier space is defined by

$$\chi(q, \omega_m) = \iint dx d\tau \chi(x, \tau) e^{-iqx+i\omega_m \tau}, \quad (22)$$

where  $\chi(x, \tau) = -\langle T_\tau O(x, \tau) O^\dagger \rangle$  is the two-particle correlation function. At small  $q$  and  $\omega$ , the dynamic magnetic susceptibility (or compressibility) can be calculated using the spin (charge) operator  $O = (\sigma_+ + \sigma_-)/\sqrt{2}$  ( $O = (\rho_+ + \rho_-)/\sqrt{2}$ ) and (15), with the result after analytic continuation

$$\chi_\nu(q, i\omega_m \rightarrow \omega + i0^+) = -\frac{1}{\pi u_\nu} \sum_p \frac{pu_\nu q}{\omega - pu_\nu q} + i\pi \sum_p q\delta(\omega - pu_\nu q) \quad (23)$$

for both branches at zero temperature. The simple pole structure of the real part of this expression is analogous to the one found for acoustic phonons. Correspondingly, the absence of damping shown by the imaginary part emphasizes once more that spin and charge acoustic excitations are eigenstates of the system. In the static ( $\omega = 0$ ) and uniform ( $q \rightarrow 0$ ) limits,  $\chi_\nu \rightarrow 2(\pi u_\nu)^{-1}$ . A non-zero susceptibility at zero temperature then occurs despite the absence of density of states at the Fermi level. The proportionality between the uniform response and the density of states that holds for a Fermi liquid is meaningless for a Luttinger liquid due to the absence of quasi-particles. The finite uniform response rather probes the density of states of acoustic boson modes in the spin or charge channel. At non zero temperature for the TL model,  $\chi_\nu(T)$  is only very weakly temperature dependent on the scale of the Debye energy  $\omega_\nu = u_\nu \alpha_0^{-1}$  of acoustic modes, which is of the order of the Fermi energy for not too large couplings.[17,18]

Other quantities like staggered density-wave (close to wave vector  $2k_F$ ) responses are also of practical importance in the analysis of X-ray and NMR experiments.[19,20,21,22] In the following we will focus on spin-spin correlation function for  $q \sim 2k_F$ ; the latter can be evaluated using the spin-density operator  $\mathbf{O} = \psi_- \boldsymbol{\sigma} \psi_+$  in the definition of the two-particle correlation function given above. At equal-time for example, one gets the power law decay

$$\begin{aligned} \chi(x) &= \langle \mathbf{O}(x) \cdot \mathbf{O}(0) \rangle \\ &\sim \frac{\cos(2k_F x)}{x^{1+K_\rho}}, \end{aligned} \quad (24)$$

which is governed by the LL parameter  $K_\rho$ . The temperature dependence of the antiferromagnetic response is given by the Fourier transform of  $\chi(x, \tau)$  evaluated at  $2k_F$  and in the static limit

$$\chi(2k_F, T) \sim T^{-\gamma}. \quad (25)$$

The power law exponent  $\gamma = 1 - K_\rho > 0$  is non universal and increases with the strength of interactions up to its highest value  $\gamma = 1$  corresponding to the Heisenberg universality class. A similar expression is found for the  $2k_F$  charge-density-wave response in the TL model. For attractive couplings, a power law singularity is to be found in the superconducting channel, where  $K_\rho$  in (24-25) is simply replaced by  $1/K_\rho$ .

The imaginary part  $\text{Im}\chi(q + 2k_F, \omega)$  of the dynamic response is another related quantity that plays an important part in experimental situations giving

an experimental access to the Luttinger liquid parameter  $K_\rho$ .[20,22] In the spin-density-wave channel of a Luttinger liquid at non zero temperature, one has the power law enhanced form

$$\text{Im}\chi(q + 2k_F, \omega) \sim (\pi u_\sigma)^{-1} \frac{\omega}{T} \left( \frac{T}{E_F} \right)^{-\gamma} \quad (26)$$

for small (real) frequency and  $q$  close to 0. We shall revert to this below in the context of NMR.

## 2.4 The one-dimensional electron gas model

When large momentum transfer ( $\sim 2k_F$ ) is allowed for scattering events, we have an additional coupling parameter which is the backscattering process denoted  $g_1$ . Moreover, when the band is half-filled (one electron per lattice site),  $4k_F$  coincides with the reciprocal lattice vector  $G = 2\pi/a$  ( $a \sim \alpha_0$  is the lattice constant) and Umklapp scattering becomes possible. Another coupling  $g_3$  is then added to the Hamiltonian for which two electrons are transferred from one side of the Fermi surface to the other. The total Hamiltonian, known as the 1D fermion gas problem now becomes  $H = H_{TL} + H'$ , where

$$\begin{aligned} H' = & \frac{1}{L} \sum_{\{k, q, \alpha\}} g_1 a_{+, k_1 + 2k_F + q, \alpha}^\dagger a_{-, k_2 - 2k_F - q, \alpha'}^\dagger a_{+, k_2, \alpha'} a_{-, k_1, \alpha} \\ & + \frac{1}{2L} \sum_{\{p, k, q, \alpha\}} g_3 a_{p, k_1 + p(2k_F + q), \alpha}^\dagger a_{p, k_2 - p(2k_F + q) + pG, -\alpha}^\dagger a_{-p, k_2, -\alpha} a_{-p, k_1, \alpha} \end{aligned} \quad (27)$$

corresponds to the additional terms expressed in the fermion representation. In terms of phase variables, the part for antiparallel spins reads

$$H' = \int dx \left\{ \frac{2g_1}{(2\pi\alpha_0)^2} \cos(\sqrt{8}\phi_\sigma) + \frac{2g_3}{(2\pi\alpha_0)^2} \cos(\sqrt{8}\phi_\rho) \right\}, \quad (28)$$

whereas the parallel part of  $g_1$  goes into an additional renormalization of  $u_\sigma$  and  $K_\nu$  in  $H_{TL}$ . From this expression, one first observes that  $g_1$  ( $g_3$ ) solely depends on the spin (charge) phase variable. Therefore the spin and charge parts of the total Hamiltonian  $H = H_\sigma + H_\rho$  still commute and thus preserve spin-charge separation.

An exact solution of  $H$  cannot be found in the general case, except at a particular value of the coupling constants for each sector, corresponding to the Luther-Emery solutions [23,3]. However, one can seek an approximate solution using scaling theory. In the framework of the Tomanaga-Luttinger model, we have already emphasized that anomalous dimensions found in single and pair correlation functions are hallmarks of scaling. In effect, a Luttinger liquid is a self-similar system when it is looked at different length  $x$  (and  $u_\nu\tau$ ) scales. We can profit by this property for the more general Hamiltonian by looking at the evolution or the flow of the couplings  $g_{1,3}$  and Luttinger liquid parameters

as a function of successive change of space and time scales. In practice, the corresponding space-time variations of the phase variables  $\phi_\nu$  are integrated out using  $g_{1,3}$  as perturbations. Then by rescaling both the initial length ( $x \rightarrow xe^{-l}$ ) and time ( $u_\nu \tau \rightarrow u_\nu \tau e^{-l}$ ) scales yields the renormalization group flow equations

$$\begin{aligned} \frac{dK_\nu}{dl} &= -\frac{1}{2}K_\nu^2 g_\nu^2 \\ \frac{dg_\nu}{dl} &= g_\nu(2 - 2K_\nu) \end{aligned} \quad (29)$$

for spin and charge parameters, where  $g_\sigma \equiv g_1$  and  $g_\rho \equiv g_3$ . In the repulsive case, where  $g_{i=1\dots 4} > 0$ ,  $g_1$  is marginally irrelevant in the spin sector, that is to say  $g_1^* \rightarrow 0$  when  $l \rightarrow \infty$ . For a rotationally invariant system, we have  $K_\sigma^* \rightarrow 1$  and  $u_\sigma^* \rightarrow v_\sigma = v_F(1 - g_4/2\pi v_F)$ . If the band filling is incommensurate,  $g_3 = 0$  and we recover in this repulsive case the physics of a Luttinger liquid for both spin and charge at large distance. At half-filling, however,  $g_3$  is non zero at  $l = 0$  and becomes a marginally relevant coupling that scales to large values as  $l$  grows; in turn, the charge stiffness  $K_\rho \rightarrow 0$  and velocity  $u_\rho^* \rightarrow 0$  at large  $l$ . Strong coupling in  $g_3$  and vanishing  $K_\rho$  signals the presence of a charge gap,[2] which is given by

$$\Delta_\rho \sim E_F \left( \frac{g_3}{E_F} \right)^{1/[2(1-n^2 K_\rho)]}, \quad (30)$$

where  $n = 1$  at half-filling. The physics here corresponds to the one of a 1D Mott insulator.[24] The presence of a gap is also confirmed by the fact that when  $l$  increases  $K_\rho$  decreases and the combination of  $2g_2(l) - g_1(l)$  will invariably crosses the so-called Luther-Emery line at  $2g_2(l_{LE}) - g_1(l_{LE}) = 6/5$ , where an exact diagonalization of the charge Hamiltonian  $H_\rho$  can be carried out.[23,3]

A charge gap is not limited to half-filling but may be present for other commensurabilities too.[2] At quarter-filling for example, the transfer of four particles from one side of the Fermi surface to the other leads (instead of the above  $g_3$  term) to the Umklapp coupling

$$H_{1/4} \simeq \frac{2g_{1/4}}{(2\pi\alpha_0)^2} \int dx \cos(2\sqrt{8}\phi_\rho). \quad (31)$$

The scaling dimension of the operator  $e^{i2\sqrt{8}\phi_\rho}$  is now  $8K_\rho$ , while each term of  $H_{TL}$  in (13) has a scaling dimension of 2, so that the flow equation becomes

$$\frac{dg_{1/4}}{dl} = (2 - 8K_\rho)g_{1/4}, \quad (32)$$

which goes to strong coupling if  $K_\rho < 1/4$ , which corresponds to sizeable couplings with longer spatial range.[25] The value of the insulating gap is given by (30) by taking  $n = 2$  at quarter-filling.[2,25] It is worth noting that in the special situation where the quarter-filled chains are weakly dimerized, both half-filling and quarter-filling Umklapp are present with different bare amplitudes – a situation met in some charge transfer salts.[26,27]

Let us look at the consequences of a charge gap on correlation functions. In the single-particle case, we see that taking  $K_\rho \rightarrow 0$  at  $T < \Delta_\rho$  yields large  $\theta_\rho$ . Therefore the single electron coherence will become vanishingly small at large distance. Each electron is confined within the characteristic length scale  $\xi_\rho \sim v_\rho/\Delta_\rho$ , which can be seen as the size of bound electron-hole pairs of the Mott insulator. A large value of  $\theta$  alters the spectral properties by producing a gap in the spectral weight and in turn the density of states. [28,29]

The impact is different on spin-spin correlation functions. We first note that the uniform magnetic susceptibility, which uniquely depends on the spin velocity, remains *unaffected* by the charge gap, as a consequence of the spin-charge separation (see § 2.5). As regards  $2k_F$  antiferromagnetic spin correlations, their amplitude increases and shows a slower spatial decay  $\chi(x) \sim 1/x$ ; this corresponds to a stronger power law singularity in temperature  $\chi(2k_F, T) \sim T^{-1}$ .

## 2.5 A many-body renormalization group approach

Having described the basic properties of the electron gas from the bosonic standpoint, we can now proceed to its renormalization group description from the many-body point of view. Although the latter works well in weak coupling, it gives a different depth of perspective in the one-dimensional case and it proves particularly useful in the complex description of instabilities of one-dimensional electronic states when interchain coupling is included.

**Renormalization group** When we try to analyze the properties of the 1D electron gas using perturbation theory, we are faced with infrared singularities. These correspond to the logarithmically singular responses  $\chi^0 \sim \ln E_F/T$  of a free electron gas to Cooper *and*  $2k_F$  electron-hole (Peierls) pair formations. One dimension is special in that both share the same phase space. [30] Their presence with different phase relations in the electron-electron scattering amplitudes indicates that both pairings counterbalance one another by interference to ultimately yield a Luttinger liquid in leading order.

Another property of Cooper and Peierls logarithmic divergences is the lack of particular energy scale in the interval between  $E_F$  and  $T$ , a feature that signals scaling. Renormalization group ideas can be applied to the many-body formulation in order to obtain the low-energy properties of the electron gas model.[31,32] In the following, we briefly outline the momentum shell Kadanoff-Wilson approach developed in Refs.[32,33,34]. The partition function  $Z$  is first expressed as a functional integral over the fermion (Grassman) fields  $\psi$

$$Z = \iint D\psi^* D\psi e^{S^*[\psi^*, \psi]}. \quad (33)$$

In the Fourier-Matsubara space, the action  $S = S_0 + S_I$  consists of a free part

$$S_0[\psi^*, \psi] = \sum_{p,\alpha,\tilde{k}} [G_p^0(\tilde{k})]^{-1} \psi_{p,\alpha}^*(\tilde{k}) \psi_{p,\alpha}(\tilde{k}) \quad (34)$$

where

$$G_p^0(\tilde{k}) = [i\omega_n - \epsilon_p(k)]^{-1} \quad (35)$$

is the bare electron propagator with  $\tilde{k} = (k, \omega_n)$ ; and an interacting part

$$S_I[\psi^*, \psi] = -\frac{T}{2L} \sum_{\{\alpha, p, \tilde{k}\}} g_{p_1 p_2; p_3 p_4}^{\alpha_1 \alpha_2; \alpha_3 \alpha_4} \psi_{p_1, \alpha_1}^*(\tilde{k}_1) \psi_{p_2, \alpha_2}^*(\tilde{k}_2) \psi_{p_3, \alpha_3}(\tilde{k}_3) \psi_{p_4, \alpha_4}(\tilde{k}_4), \quad (36)$$

in which the couplings constants of the electron gas model are  $g_{+-;+-}^{\alpha\alpha';\alpha'\alpha} = g_1$ ,  $g_{+-;-+}^{\alpha\alpha';\alpha'\alpha} = g_2$ ,  $g_{\pm\pm;\mp\mp}^{\alpha\alpha';\alpha'\alpha} = g_3$ , and  $g_{\pm\pm;\pm\pm}^{\alpha\alpha';\alpha'\alpha} = 2g_4$ .[35] The relevant parameter space of the action for the electron gas will be denoted

$$\mu_S = (G_p^0, g_1, g_2, g_3, g_4). \quad (37)$$

The RG tool is used to look at the influence of high-energy states on the electron-electron scattering near  $\pm k_F$  at low energy. We will focus on the RG results at the one-loop level, which will be sufficient for our purposes. The method consists of successive partial integrations of fermion degrees of freedom ( $\bar{\psi}^{(*)}$ ) in the outer energy shell (o.s)  $\pm E_0(\ell) d\ell/2$  above and below the Fermi points as a function of  $\ell$ .[32] Here  $E_0(\ell) = E_0 e^{-\ell}$  with  $\ell > 0$ , is the scaled bandwidth cutoff  $E_0 (\equiv 2E_F)$  imposed to the spectrum (1). We can write

$$\begin{aligned} Z \sim & \int \int_{<} D\psi^* D\psi e^{S[\psi^*, \psi]_\ell} \int \int_{\text{o.s}} D\bar{\psi}^* D\bar{\psi} e^{S_0[\bar{\psi}^*, \bar{\psi}]} e^{S_{I,2} + \dots} \\ & \propto \int \int_{<} D\psi^* D\psi e^{S[\psi^*, \psi]_\ell + \frac{1}{2}\langle S_{I,2}^2 \rangle_{\text{o.s}}} + \dots, \end{aligned} \quad (38)$$

where  $S_{I,2}$  is given by the interaction term with two  $\bar{\psi}^{(*)}$  in the outer momentum shell in the Cooper and Peierls channels (2 $k_F$  electron-hole and zero momentum Cooper pairs), while the other two remain fixed in the inner (<) shell.

At the one-loop level, the averages  $\langle (S_{I,2})^2 \rangle_{\text{o.s}}$  in the outer momentum shell are calculated with respect to  $S_0[\psi^*, \psi]$ , which ultimately leads to the scaling transformation of  $\mu_S$  as a function of  $\ell$

$$\mathcal{R}_{d\ell}[\mu_S(\ell)] = \mu_S(\ell + d\ell). \quad (39)$$

The outer momentum shell contributions to the Peierls and Cooper channels have different signs and lead to the aforementioned interference in the renormalization flow, which is governed by the following set of equations

$$\begin{aligned} \frac{d\tilde{g}_1}{d\ell} &= -\tilde{g}_1^2 + \dots \\ \frac{d}{d\ell}(2\tilde{g}_2 - \tilde{g}_1) &= \tilde{g}_3^2 + \dots \\ \frac{d\tilde{g}_3}{d\ell} &= \tilde{g}_3(2\tilde{g}_2 - \tilde{g}_1) + \dots, \end{aligned} \quad (40)$$

where the influence of  $g_4$  has been included through the normalization  $\tilde{g}_1 = g_1/\pi v_\sigma$ ,  $2\tilde{g}_2 - \tilde{g}_1 = (2g_2 - g_1)/\pi v_\rho$ , and  $\tilde{g}_3 = g_3/\pi v_\rho$ . These scaling equations,[35]

are consistent with those obtained in (29) from the bosonization technique by expanding the stiffness constants  $K_{\nu=\sigma,\rho}$  to leading order in the coupling constants. Therefore from the many-body standpoint, the interference between the Cooper and Peierls channels appears as an indispensable building block of Luttinger and Luther-Emery liquids.

**Magnetic susceptibility** The description sketched above can also be used for the calculation of uniform responses at small  $q$  and  $\omega$  when the couplings  $g_1$  and  $g_3$  are present.[21,35,17] We will be mainly concerned here with the spin susceptibility (a similar approach also applies for compressibility). We will see that the flow of  $g_1(\ell)$  is responsible for a temperature dependence of susceptibility.

The first thing that needs to be said is that thermally excited spin excitations involved in the uniform magnetic response do not contribute to the logarithmic singularities of the Cooper and Peierls channels. In effect, these last singularities refer to electron and hole states located outside the thermal width  $\sim 2T$  around the Fermi points, while it is the other way around for the uniform spin response of the Landau channel. The fact that the Landau channel does not interfere directly with the other two constitutes an advantage in the calculation. One can indeed use the renormalization group method to first integrate quantum degrees in the interfering Cooper and Peierls channels, namely down to  $\ell_T = \ln E_F/T$ , after which the resulting low-energy action can be used to calculate uniform spin susceptibility.[21,17] If we try to outline this way of doing, we first note that the interacting part of the action at  $\ell$  can be written

$$S_I = \sum_{p,\tilde{q}} (2g_2 - g_1)(\ell) \rho_p(\tilde{q}) \rho_{-p}(-\tilde{q}) - g_1(\ell) \sum_{p,\tilde{q}} \mathbf{S}_p(\tilde{q}) \cdot \mathbf{S}_{-p}(-\tilde{q}) + S_I[g_4], \quad (41)$$

in which we have defined the composite fields  $\rho_{\pm} = \frac{1}{2}(L)^{-\frac{1}{2}} \sum_{k^*,\alpha} \psi_{\pm,\alpha}^* \psi_{\pm,\alpha}$  for charge and  $\mathbf{S}_{\pm} = \frac{1}{2}(L)^{-\frac{1}{2}} \sum_{k^*,\alpha} \psi_{\pm,\alpha}^* \boldsymbol{\sigma}^{\alpha\beta} \psi_{\pm,\beta}$  for spin. Here the sum on  $k$  satisfies  $|\epsilon_p(k)| \leq E_0(\ell)/2$ ; we have omitted the  $g_3$  term since it gives no direct contribution to the Landau channel. The above expression for the action being quadratic in spin and charge fields, it can be linearized using an Hubbard-Stratonovich transformation which allows us to express the partition function as a functional integral over auxiliary charge  $\phi$  and spin  $\mathbf{M}$  fields

$$Z = Z(g_4) \iint \mathcal{D}\phi \mathcal{D}\mathbf{M} \exp \left\{ - \sum_{\tilde{q},p,p'} [\phi_p(\tilde{q}) A_{p,p'}(\tilde{q}) \phi_{p'}(-\tilde{q}) + \mathbf{M}_p(\tilde{q}) B_{p,p'}(\tilde{q}) \mathbf{M}_{p'}(-\tilde{q})] \right\}, \quad (42)$$

where  $Z(g_4)$  is the partition function of the system with  $g_4$  interaction only, which can be treated in RPA in the spin and charge sectors.[18] The effective low-energy free energy density is thus essentially quadratic in both  $\phi$  and  $\mathbf{M}$  – mode-mode coupling terms vanish for a linear spectrum – and can be seen as an approximate harmonic representation of the electron gas model at low energy.

From the expressions of matrix elements  $A_{p,p}(\tilde{q}) = \frac{1}{2}(2\tilde{g}_2 - \tilde{g}_1)(\ell)$ ,  $A_{\pm,\mp} = 1$  and  $B_{\pm,\pm}(\tilde{q}) = -\frac{1}{2}\tilde{g}_1(\ell)$ ,  $B_{\pm,\mp} = 1$ , the uniform magnetic response, when expressed as statistical averages over auxiliary fields, is given by

$$\begin{aligned}\chi_\sigma(\tilde{q}) &= \frac{1}{g_1(\ell)} \left[ \left( \frac{1}{6} \sum_{p,p'} \mathbf{M}_p(\tilde{q}) \cdot \mathbf{M}_{p'}(-\tilde{q}) \right) - 1 \right] \\ &= -\frac{2}{\pi} \frac{1}{\bar{u}_\sigma(\ell)} \frac{u_\sigma^2(\ell)q^2}{[\omega - u_\sigma(\ell)q][\omega + u_\sigma(\ell)q]} \\ &\quad + i \frac{1}{\bar{u}_\sigma(\ell)} \sum_p u_\sigma(\ell)q \delta(\omega - pu_\sigma(\ell)q),\end{aligned}\quad (43)$$

where  $\bar{u}_\sigma(\ell) = v_\sigma(1 + \frac{1}{2}\tilde{g}_1(\ell))$ . The spectrum of low energy acoustic spin excitations now becomes

$$\begin{aligned}\omega_\sigma &= u_\sigma(\ell) | q | \\ &= v_\sigma \left( 1 - \tilde{g}_1^2(\ell)/4 \right)^{\frac{1}{2}} | q |,\end{aligned}\quad (44)$$

which, owing to the presence of  $g_1$ , shows  $\ell$  dependent corrections with respect to the Tomanaga-Luttinger limit (Eqn.(10)) (a similar expression holds for the charge spectrum following the substitution  $v_\sigma \rightarrow v_\rho$  and  $-\tilde{g}_1(\ell) \rightarrow (2\tilde{g}_2 - \tilde{g}_1)(\ell)$ ). The temperature dependence of the static and uniform spin susceptibility is obtained by putting  $\tilde{q} = 0$  and  $\ell \rightarrow \ln \omega_\sigma/T$  in (44) with the result

$$\chi_\sigma(T) = \frac{2}{\pi v_\sigma} \frac{1}{1 - \frac{1}{2}\tilde{g}_1(T)}, \quad (45)$$

where

$$\tilde{g}_1(T) = \frac{\tilde{g}_1}{1 + \tilde{g}_1 \ln \omega_\sigma/T} \quad (46)$$

is the solution of the first equation of (40). For repulsive couplings, the reduction of  $g_1(T)$  imparts a temperature dependence to the susceptibility which is shown in Fig. 1. As one can see, the logarithmic corrections make the  $\chi$  approaching its  $T = 0$  value with an infinite slope.[35,21,17,36] This singularity in the derivative occurs only at very low temperature and can be hard to detect in practice. Finite magnetic field or interchain hopping between stacks tends to suppress the singularity.

**Nuclear relaxation rate** The nuclear spin-lattice relaxation rate measured in NMR experiments is another quantity of practical importance if one tries to gain information about spin correlations. It is given by the Moriya expression

$$T_1^{-1} = |A|^2 T \int \frac{\chi''(\mathbf{q}, \omega)}{\omega} d^D q, \quad (47)$$

which is taken in the zero Larmor frequency limit ( $\omega \rightarrow 0$ ) and where  $A$  is proportional to the hyperfine matrix element. Thus the relaxation of nuclear

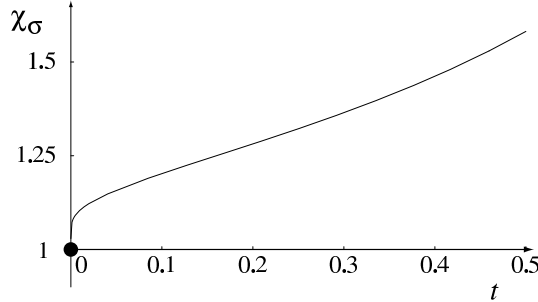


**Fig. 1.** The temperature variation of the magnetic susceptibility expressed in  $\pi v_\sigma/2$  units as a function of the reduced temperature  $t = T/\omega_\sigma$  for the electron gas model ( $\tilde{g}_1 \sim 1$ ).

spins gives in principle relevant information about the static, dynamics and dimensionality  $D$  of electronic spin correlations. This gives in turn a relatively easy access to the parameters  $K_\rho$ ,  $\bar{u}_\sigma(T)$  and  $u_\sigma(T)$  of the electron gas.[37] According to Eqns. (43) and (26), the enhancements of  $\chi''$  occur at  $q \sim 0$  and in the interval  $q \sim 2k_F \pm T/v_F$  close to  $2k_F$ . The integration is then readily done to give

$$T_1^{-1} \simeq C_0(T)T\chi_\sigma^2(T) + C_1(T)T^{K_\rho}. \quad (48)$$

Owing to the presence of  $g_1$ , we have  $C_0(T) = C_0(u_\sigma(T)/\bar{u}_\sigma(T))^{\frac{1}{2}}$  and  $C_1(T) = C_1(1 + \tilde{g}_1 \ln \omega_\sigma/T)^{\frac{1}{2}}$ . As a function of temperature, two different behaviors can be singled out. At high temperature, where uniform spin correlations dominate and the  $2k_F$  ones are small, the relaxation rate is then governed by the  $C_0(T)T\chi_\sigma^2(T)$  term. In the low temperature domain, however,  $2k_F$  spin correlations are singularly enhanced while uniform correlations remain finite so that  $T_1^{-1} \sim C_1(T)T^{K_\rho}$ . The temperature dependence of  $T_1^{-1}$  over the whole temperature range thus contrasts with that of a Fermi liquid where  $(T_1 T)^{-1} \sim \text{cst.}$ , as found for the Korringa law in ordinary metals.

It is interesting to consider the case where a gap is present in the charge part and for which  $K_\rho = 0$ . We thus have

$$T_1^{-1} \simeq C_0(T)T\chi_\sigma^2(T) + C_1(T). \quad (49)$$

The relaxation will tend to show a finite intercept as  $T \rightarrow 0$  (here logarithmic corrections in  $C_1(T)$  will give rise to an upturn in the low temperature limit). The temperature profile is summarized in Figure 2.

### 3 Instabilities of 1D quantum liquids: interchain coupling

Electronic materials like organic conductors can be only considered as close realizations of 1D interacting fermion systems. In the solid state, molecular stacks are not completely independent, that is to say *interchain coupling*, though small,

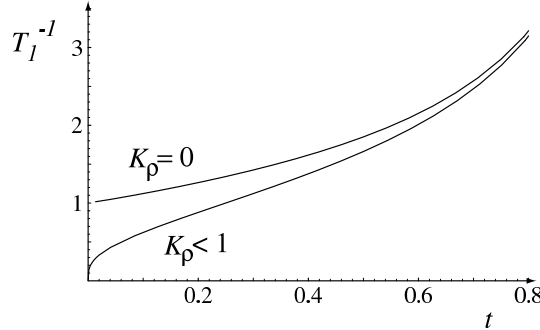


**Fig. 2.** Nuclear spin-lattice relaxation rate (expressed in arbitrary units) as a function of the reduced temperature  $t = T/\omega_\sigma$ , when the system scales to the Luttinger liquid ( $1 > K_\rho > 0$ ) and strong coupling ( $K_\rho = 0$ ) sectors.

must be taken into account in their description. Two different kinds of interchain coupling are generally considered. First, we have potential coupling like Coulomb interaction which introduces scattering of particles on different stacks. In certain conditions, potential coupling may give rise to long-range (density-wave) order at finite temperature. Second, there is the kinetic coupling, commonly denoted  $t_\perp$ , which allows an electron to hop from one stack to another. In the following, we shall confine ourselves to the latter coupling, which is the most studied and by far the most complex. In effect, it is from  $t_\perp$  that most instabilities of 1D quantum liquids discussed thus far can occur. These are also called *crossovers* which form the links between the physics in one and higher dimensions as either the restoration of a Fermi liquid component or the onset of long-range order. In the following, we will review the physics of both types of crossover induced by  $t_\perp$  using the renormalization group method that was described earlier.

### 3.1 One-particle dimensionality crossover and beyond

**The route towards the restoration of a Fermi liquid** The overlap of molecular orbitals allowing electrons to hop from one chain to the next modifies the electron spectrum. In the tight-binding picture of a linear array of  $N_\perp$  chains we have

$$E_p(\mathbf{k}) = \epsilon_p(k) - 2t_\perp \cos k_\perp, \quad (50)$$

where  $\mathbf{k} = (k, k_\perp)$ . Generalizing the functional-integral representation of the partition function in the presence of a non-zero but small  $t_\perp \ll E_F$ , the propagator of the free part of the action is now  $G_p^0(\mathbf{k}, \omega_n) = [i\omega_n - E_p(\mathbf{k})]^{-1}$ . The non-interacting situation can trivially serve to illustrate how a dimensionality crossover of the quantum coherence in the single-particle motion is achieved as a function of temperature. We first note that since  $t_\perp$  enters on the same footing as  $\omega_n$  (or  $T$ ) and  $\epsilon_p$  (or  $k$ ) in the bare propagator, it is a relevant perturbation; that is to say its importance grows according to  $t'_\perp = st_\perp$  following the rescaling of energy  $\epsilon'_p = s\epsilon_p$  and temperature  $T' = sT$  by a factor  $s > 1$ . The temperature

scale at which the crossover occurs can be readily obtained by equating  $s$  with the ratio of length scales  $\xi/a$  and by setting  $t'_\perp \sim E_F$  at the crossover. This condition of isotropy yields the crossover temperature  $T_{x^1} \sim t_\perp$ , which is not a big surprise since  $t_\perp$  acts as the only characteristic energy scale introduced in the interval between  $T$  and  $E_F$ .

In the presence of interactions, however, the flow of the enlarged parameter space  $\mu_S = (G_p^0(k, \omega_n), t_\perp, g_1, g_2, g_3)$  of the action, under the transformation (39) will modify this result. As shown in great detail elsewhere,[32,34] the partial trace operation (38), when carried out beyond the one-loop level, not only alters the scattering amplitudes but also the single-particle propagator. At sufficiently high energy, the corresponding one-particle self-energy corrections keep in first approximation their 1D character and then modify the purely one-dimensional part of the propagator through the renormalization factor  $z(\ell)$ . Thus the effective bare propagator at step  $\ell$  reads

$$G_p^0(\mathbf{k}, \omega_n, \mu_S(\ell)) = \frac{z(\ell)}{i\omega_n - \epsilon_p(k) + 2z(\ell)t_\perp \cos k_\perp}. \quad (51)$$

Detailed calculations show that  $z(\ell)$  obeys a distinct flow equation at the two-loop level which depends on the couplings constants (the generalization of Eqn. (40) at the two-loop level).[32] Its integration up to  $\ell_T$  leads to

$$z(T) \sim \left( \frac{T}{E_F} \right)^\theta, \quad (52)$$

where the exponent  $\theta > 0$  for non-zero interaction and is consistent with the one given by the bosonization method (cf. Eq. (21)) in lowest order. Being the residue at the single-particle pole of the 1D propagator,  $z(T)$  coincides with the reduction factor of the density of states at the Fermi level (Eqn. (21)). The reduction of the density of states along the chains also modifies the amplitude of interchain hopping. The crossover criteria mentioned above now becomes  $(\xi/a)z(T)t_\perp \sim E_F$ , which leads to the usual downward renormalization of the one-particle crossover temperature:[38]

$$T_{x^1} \sim t_\perp \left( \frac{t_\perp}{E_F} \right)^{(1-\theta)/\theta}. \quad (53)$$

According to this expression,  $T_{x^1}$  decreases when the interaction – which can be parametrized by  $\theta$  – increases (Figure 3); it is non-zero as long as  $\theta < 1$  for which  $t_\perp$  remains a relevant variable. The system then undergoes a crossover to the formation of a Fermi liquid with quasi-particle weight  $z(T_{x^1})$ . For strong coupling,  $T_{x^1}$  vanishes at the critical value  $\theta_c = 1$  and becomes undefined for  $\theta > 1$ ,  $t_\perp$  being then marginal in the former case and irrelevant in the latter (Figure 3). Consequently, in the latter case, no transverse band motion is possible and the single-particle coherence is spatially confined along the stacks. These large values of  $\theta$  cannot be attained from the above perturbative renormalization group. They are found on the Luther-Emery line at half-filling or at quarter-filling in the presence of a charge gap;[3,28,25] in the gapless Tomanaga-Luttinger

model for sufficiently strong coupling constants or when the range of interaction increases.[7]

The above scaling approach to the deconfinement temperature is obviously not exact and corresponds to a random phase approximation with respect to the transverse one-electron motion.[38,39,40] This can be seen easily by just rewriting (51) in the RPA form

$$G_p^0(\mathbf{k}, \omega_n, \mu_S(\ell)) = \frac{z(\ell)G_p^0(k, \omega_n)}{1 + z(\ell)G_p^0(k, \omega_n) 2t_\perp \cos k_\perp}, \quad (54)$$

where  $z(\ell)G_p^0(k, \omega_n)$  is the 1D propagator at the step  $\ell$  of the RG. Transverse RPA becomes essentially exact, however, in the limit of infinite range  $t_\perp$ .[39] In regard to this approximation, it should be stressed that the above renormalization group treatment of deconfinement does not take into account the dynamics of spin-charge separation, namely the fact that the spin and charge excitations travel at different velocities (§ 2.1). It was inferred that this mismatch in the kinematics may suppress  $T_{x^1}$  and in turn the formation of a Fermi liquid.[41] As shown by Boies *et al.*[39] using a functional-integral method, the use of the Matsubara-Fourier transform of the complete expression (16) in the RPA allows one to overcome this flaw of the RG. However, the calculation shows that in the general case it still yields a finite crossover temperature

$$T_{x^1} \approx t_\perp \left( \frac{t_\perp}{E_F} \right)^{\theta/(1-\theta)} \left( \frac{v_F}{u_\rho} \right)^{\theta_\rho/(1-\theta)} \left( \frac{v_F}{u_\sigma} \right)^{\theta_\sigma/(1-\theta)} F[(u_\sigma/u_\rho)^{1/2}], \quad (55)$$

where  $F(x)$  is a scaling function. Distinct velocities for spin and charge do give rise to additional corrections but the difference takes place at the quantitative level. Electronic deconfinement is therefore robust at this level of approximation and even beyond.[42,43,44,40,45,46] It is worth stressing that the renormalization of  $t_\perp$  by intrachain interactions has been recently confirmed on numerical grounds for two-chain (ladder) fermion systems. [47,48]

As we will see later, the above picture is modified significantly when the influence of  $t_\perp$  on pair correlations is taken into account, especially when the amplitude of interactions increases and  $T_{x^1}$  becomes small. As regards the temperature interval over which one-particle crossover is achieved, it is not expected to be very narrow. In comparison with crossovers in ordinary critical phenomena, which are confined to the close vicinity of a phase transition,[49] deconfinement of single-particle coherence in quasi-1D system is likely to be spread out over a sizeable temperature domain. This is so because the temperature interval  $\sim [T, E_F]$  of the 1D quantum critical domain, which is linked to the primary Luttinger liquid fixed point, is extremely large. Recent calculations using dynamical mean-field theory seem to corroborate the existence of a sizeable temperature interval for the crossover.[45]

**Instability of the Fermi liquid** Let us now turn our attention to the question of whether or not a Fermi liquid component in a quasi-one-dimensional metal

remains stable well below  $T_{x^1}$ . Here we will neglect all the aforementioned transients to deconfinement and consider  $T_{x^1}$  as a sharp boundary between the Luttinger and Fermi liquids. By looking at the effective spectrum of the above model in which  $t_\perp \rightarrow t_\perp^* = zt_\perp$  in (50), we observe that the whole spectrum obeys the relation  $E_-^*(\mathbf{k}) = -E_+^*(\mathbf{k} + \mathbf{Q}_0)$ , showing electron-hole symmetry or perfect nesting at  $\mathbf{Q}_0 = (2k_F, \pi)$ . The response of the free quasi-1D electron gas is still logarithmically singular  $\chi^0(\mathbf{Q}_0, T) \sim \ln T_{x^1}/T$  in the Peierls channel for  $\mathbf{Q}_0$  electron-hole excitations within the energy shell  $\sim T_{x^1}$  above and below the coherent *warped* Fermi surface. This singularity is also to be found in the perturbation theory of the scattering amplitudes, and can therefore lead to an instability of the Fermi liquid. For repulsive interactions, the most favorable instability is the one that yields a spin-density-wave state. The temperature at which the SDW instability occurs can be readily obtained by extending the renormalization group method of § 2.5 below  $T_{x^1}$  (or  $\ell > \ell_{x^1} = \ln E_F/T_{x^1}$ ). When perfect nesting prevails, a not too bad approximation consists of neglecting the interference between the Cooper and Peierls channels [50] (we shall revert to the problem of interference below  $T_{x^1}$  later in § 4.1). Thus by retaining the outer shell decomposition of  $S_{I,2}$  in the latter channel only, one can write down a ladder flow equation

$$\frac{d\tilde{J}}{d\ell} = \frac{1}{2}\tilde{J}^2 + \dots \quad (56)$$

for an effective coupling constant  $\tilde{J} = \tilde{g}_2 + \tilde{g}_3 - \tilde{V}_\perp \dots$  that defines the net attraction between an electron and a hole separated by  $\mathbf{Q}_0$  (the origin of the exchange term  $V_\perp$  will be discussed in § 3.2). This equation is integrated at once

$$\tilde{J}(T) = \frac{\tilde{J}^*}{1 - \frac{1}{2}\tilde{J}^* \ln T_{x^1}/T}, \quad (57)$$

where  $\tilde{J}^*$  is the effective SDW coupling at  $T_{x^1}$ , resulting from the integration of 1D many-body effects at  $\ell < \ell_{x^1}$ . The above expression leads to a simple pole singularity at the temperature scale

$$T_c = T_{x^1} e^{-2/\tilde{J}^*}, \quad (58)$$

which corresponds to a BCS type of instability of the Fermi liquid towards a SDW state. As long as the nesting conditions are fulfilled, it invariably occurs for any non-zero interaction (dashed line of Fig. 3).

Nesting frustration is therefore required to suppress the transition. When nesting deviations are sufficiently strong, we will see, however, that the Fermi liquid is not stabilized after all. Actually, when interference between the Peierls and the Cooper channels is restored, the system turns out to become unstable to superconducting pairing, a mechanism akin to the Kohn-Luttinger mechanism for superconductivity in isotropic systems. [51,52,53,54,55] We shall return to this in § 4.1.

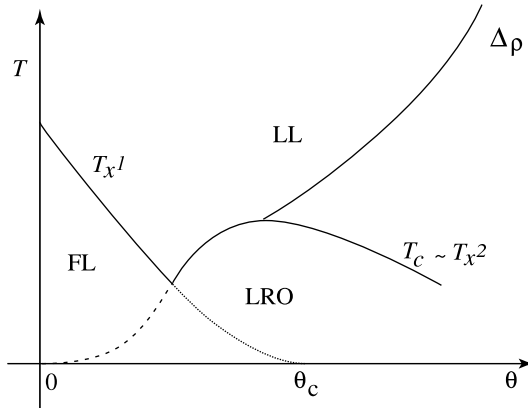


**Fig. 3.** Characteristic temperature scales of the quasi-one-dimensional electron gas model as a function of interaction, parametrized by the exponent  $\theta$ . In the Fermi liquid sector, perfect nesting conditions prevail.

### 3.2 Two-particle dimensionality crossover and pair deconfinement

When one examines the properties of the one-dimensional electron gas, one observes that the exponent  $\gamma$  of the pair response is not simply equal to twice the anomalous dimension  $\theta$  of the single-particle Green's function. Although both exponents depend on the Luttinger liquid parameter  $K_\rho$ , one-electron and pair correlations are governed by distinct power law decays. Thus the effect of an increase in the strength of interaction ( $K_\rho$  is decreasing for repulsive interactions) leads to a faster spatial decay of single particle coherence (Eqn. (17)), whereas the opposite is true for triplet electron-hole pair (antiferromagnetic) correlations (Eq. (24)). The question now arises whether  $t_\perp$  can promote interchain pair propagation besides single-particle coherence. Actually, this possibility exists and results from *interchain pair-hopping* processes,[56,57,58] a mechanism that is not present in the Hamiltonian at the start but which emerges when interactions along the stacks combine with  $t_\perp$  in the one-dimensional region. The renormalization group approach proved to be particularly useful in this respect making possible a unified description of both modes of propagation. [56,54,32,33,34]

For repulsive interactions, the most important pair hopping contribution is the interchain exchange which favors antiferromagnetic ordering of neighboring chains. Roughly speaking, from each partial trace operation in (38), there is a ‘seed’  $f(\ell)d\ell$  of interchain exchange that builds up as a result of combining perturbatively the effective hopping ( $zt_\perp$ ) and the couplings ( $g$ ’s) in the shell of degrees of freedom to be integrated out. This can be seen as a new relevant interaction for the system, which in its turn is magnified by antiferromagnetic correlations. The net interchain exchange term generated by the flow of renormalization can be written as

$$S_\perp = -\frac{1}{4} \sum_{\langle i,j \rangle} \sum_{\tilde{q}} V_\perp(\ell) \mathbf{O}_i(\tilde{q}) \cdot \mathbf{O}_j(\tilde{q}), \quad (59)$$

which favors antiferromagnetic of spins on neighboring chains  $i$  and  $j$ . Going to transverse Fourier space,  $V_{\perp}$  corresponds to the exchange amplitude at the ordering wave vector  $\mathbf{Q}_0 = (2k_F, \pi)$ . In the one-dimensional regime, it is governed at the one-loop level by the distinct flow equation

$$\frac{d}{d\ell} \tilde{V}_{\perp} = f(\ell) + \tilde{V}_{\perp} \gamma(\ell) - \frac{1}{2} (\tilde{V}_{\perp})^2, \quad (60)$$

where  $\tilde{f}(\ell) \simeq -2[(\tilde{g}_2(\ell) + \tilde{g}_3(\ell))t_{\perp}/E_0]^2 e^{(2-2\theta(\ell))\ell}$ . Here  $\theta(\ell)$  and  $\gamma(\ell)$  are the power law exponents of the one-particle propagator (Eqns.(21) and (52)) and antiferromagnetic response (Eqn. (25)) respectively (these are scale dependent due to the presence of Umklapp scattering). One observes from the right-hand-side of the above equation that the seed term resulting from the perpendicular delocalization of the electron and hole within the pair competes with the second term due to antiferromagnetic correlations along the chains. The outcome of this competition will be determined by the sign of  $2 - 2\theta(\ell) - \gamma(\ell)$ . Regarding the last term, it is responsible for a simple pole singularity of  $J_{\perp}$  at a non-zero  $\ell_c = \ln(E_F/T_c)$ , signaling the onset of long-range order at  $T_c$ [59]. The temperature at which the change from the one-dimensional regime to the onset of transverse order occurs can be equated with a distinct dimensionality crossover denoted by  $T_{x^2} \simeq 2T_c$  for pair correlations. The latter makes sense as long as  $zt_{\perp}$  is still a perturbation, that is to say for  $T_{x^2} > T_{x^1}$ , which defines the region of validity of (60).

For repulsive interactions and in the presence of relevant Umklapp scattering, one can therefore distinguish two different situations. The first one corresponds to the presence of a charge gap well above the transition. As we have seen earlier, it defines a domain of  $\ell$  where  $\theta(\ell)$  is large and  $\gamma(\ell) = 1$ , that is  $2 - 2\theta(\ell) - \gamma(\ell) < 0$ . The physics of this strong coupling regime bears some resemblance to the problem of weakly coupled Heisenberg spin chains. However, in the Luther-Emery liquid case or at quarter-filling with a gap, each electron is not confined to a single site as in the Heisenberg limit but is delocalized over a finite distance  $\xi_{\rho} \sim v_F/\Delta_{\rho}$ , corresponding to the size of bound electron-hole pairs. A simple analysis of (60) shows that these pair effectively hop through an effective coupling  $\tilde{J}_{\perp} \approx (\xi_{\rho}/\alpha_0)(t_{\perp}^{*2}/\Delta_{\rho})$ . When coupled to singular correlations along the chains, this leads to the antiferromagnetic transition temperature

$$T_c \approx \frac{t_{\perp}^{*2}}{\Delta_{\rho}} \sim T_{x^2}, \quad (61)$$

where  $t_{\perp}^{*} = z(\Delta_{\rho})t_{\perp}$  is the one-particle hopping at the energy scale of the charge gap.

A characteristic feature of strong coupling is the increase of  $T_c$  when the gap  $\Delta_{\rho}$  decreases (Fig. 3). The above behavior of  $T_c$  continues up to the point where  $T_{x^2} \sim \Delta_{\rho}$ , namely when the insulating behavior resulting from the charge gap merges into the critical domain of the transition.  $\theta$  and  $\gamma$  take smaller values in the normal metallic domain so that  $2 - 2\theta(\ell) - \gamma(\ell)$  will first reach zero after which it will become positive corresponding to interchain pair-hopping in weak

coupling. The growth of the seed term then surpasses the one due to pair vertex corrections in (60). An approximate expression of the transition temperature in this case is found to be

$$T_c \approx g^{*2} t_{\perp}^{*}, \quad (62)$$

where  $g^* = g_2^* + g_3^*$  and  $t_{\perp}^* = t_{\perp} z(T_c)$ . Again this expression makes sense as long as  $T_{x^2} > T_{x^1}$ , which on the scale of interaction should not correspond to a wide interval. Still, it is finite and shows a decrease of  $T_c$  for decreasing interactions. This leads to a maximum of  $T_c$  at the boundary between strong and weak coupling domains (Fig. 3).

As soon as  $T_{x^2} < T_{x^1}$ , the single particle deconfinement occurs first at  $zt_{\perp} \approx E_0(\ell)$  and interchain hopping can no longer be treated as a perturbation. This invalidates (60), and we have seen earlier that a Fermi liquid component forms under these conditions. An instability towards SDW is still possible under good nesting conditions for the Fermi surface. The exchange mechanism then smoothly evolves towards the condensation of electron-hole pairs from a Fermi liquid. In this regime, the residual pair-hopping amplitude  $V_{\perp}(\ell_{x^1})$  contributes to the effective coupling  $J^*$  in (58). Figure 4 summarizes the various temperature scales characterizing the quasi-one-dimensional electron gas problem in the presence of Umklapp scattering.

## 4 Applications

### 4.1 The Fabre and Bechgaard transfer salt series

The series of Fabre ((TMTTF)<sub>2</sub>X) and Bechgaard ((TMTSF)<sub>2</sub>X) transfer salts show striking unity when either hydrostatic or chemical pressure (S/Se atom or anion  $X = \text{PF}_6$ ,  $\text{AsF}_6$ ,  $\text{Br}$ , ..., substitutions) is applied. Electronic and structural properties naturally merge into the universal phase diagram depicted in Fig. 4 [60,61,62,33,63]. Its structure reveals a characteristic sequence of ground states enabling compounds of both series to be linked one to another [64,65,66,67,22,68,69,70,71,72,73]. In this way, Mott insulating sulfur compounds like (TMTTF)<sub>2</sub>PF<sub>6</sub>, AsF<sub>6</sub>... were found to develop a charge-ordered (CO) state and a lattice distorted spin-Peierls (SP) state. The SP state is suppressed under moderate pressure and replaced by an antiferromagnetic (AF) Néel state similar to the one found in the (TMTTF)<sub>2</sub>Br salt in normal conditions; the Mott state is in turn suppressed under pressure and antiferromagnetism of sulfur compounds then acquires an itinerant character analogous to the spin-density wave (SDW) state of the (TMTSF)<sub>2</sub>X series at low pressure. Around some critical pressure  $P_c$ , the SDW state is then removed as the dominant ordering and forms a common boundary with organic superconductivity which closes the sequence of ordered states.

Within the bounds of this review, we shall not attempt a detailed discussion of the whole structure of the phase diagram but rather place a selected emphasis on the description of antiferromagnetic and superconducting orderings together with their respective normal phases. A detailed discussion of the spin-Peierls instability and charge ordering can be found elsewhere.[74,33,75,19,76,73,77]

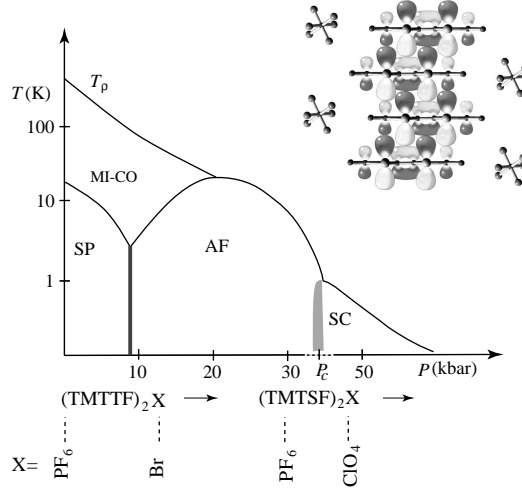


**Fig. 4.** Temperature-Pressure phase diagram of the Fabre  $((\text{TMTTF})_2\text{X})$  and Bechgaard  $((\text{TMTSF})_2\text{X})$  salts series. Inset: a side view of the crystal structure with the electronic orbitals of the stacks.

*Electrical transport and susceptibility* A convenient way to broach the description of the phase diagram is to first examine the normal phase of the Fabre salts  $(\text{TMTTF})_2\text{X}$  for the inorganic monovalent anions  $\text{X} = \text{PF}_6$  and  $\text{Br}$ . [78]. As shown in Fig. 5, there is a clear upturn in electrical resistivity at temperatures  $T_\rho \approx 220 \text{ K}$  ( $\text{PF}_6$ ) and  $T_\rho \approx 100 \text{ K}$  ( $\text{Br}$ ), which depicts a change from metallic to insulating behavior.[64] In both cases,  $T_\rho$  is a much higher temperature scale than the one connected to long-range order whose maximum is around 20 K. Below  $T_\rho$ , charge carriers become thermally activated. In a band picture of insulators, a thermally activated behavior should be present for spins too. For the compounds shown in Fig. 5, spin excitations are instead unaffected and remain gapless. This is shown by the regular temperature dependence of the spin susceptibility  $\chi_\sigma$  at  $T_\rho$  (inset of Fig. 5). Resistivity data tell us that the gap in the charge is about  $\Delta_\rho \approx 2 \dots 2.5 T_\rho$ , which exceeds the values of  $t_{\perp b}$  given by band calculations. According to the discussion given in § 3.2, this would correspond to a situation of strong electronic confinement along the chains. Confinement is confirmed by the absence of a plasma edge in the reflectivity of both compounds when the electric field is oriented along the transverse  $b$  direction.[70,79]

The magnetic susceptibility, which decreases with the temperature, is also compatible with the one-dimensional prediction of Fig. 1. Wzietek *et al.*,[22] analyzed in detail the NMR susceptibility data at constant volume using the expression (45). Very reasonable fits were obtained above 50 K provided that interactions  $g_{1,2,4} \simeq 1$  are sizeable. In the charge sector, when the origin of the gap is attributed to half-filling umklapp alone, one has for a compound like  $(\text{TMTTF})_2\text{PF}_6$  the small bare value  $\tilde{g}_3 \sim 0.1$ ; which is obtained from reasonable band parameters by matching the experimental  $T_\rho$  and the value  $\ell_\rho$  at which

$\tilde{g}_3(\ell_\rho) \sim 1$  in (40). [61,33] This is consistent with the fact that the stacks are weakly dimerized.[26,60,80] In the quarter-filling scenario,  $g_{1/4}$  would be much larger using small  $K_\rho$  in (30).

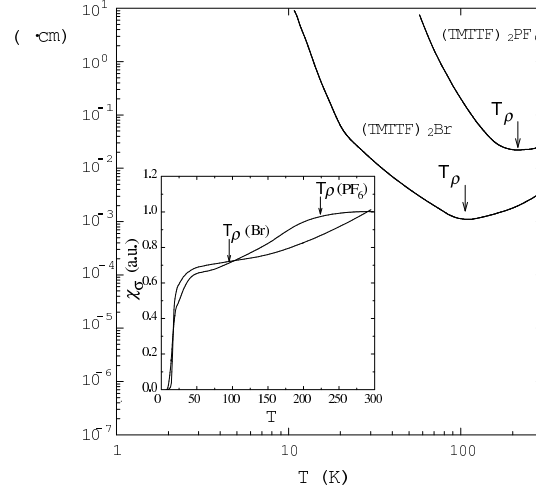


**Fig. 5.** Temperature dependence of resistivity and static spin susceptibility (inset) for the Fabre salts  $(\text{TMTTF})_2\text{Br}$  and  $(\text{TMTTF})_2\text{PF}_6$ .

*Nuclear magnetic resonance* Among other measurable quantities that are sensitive to one-dimensional physics, we have the temperature dependence of the nuclear spin-lattice relaxation rate  $T_1^{-1}$ .[22] Consider for example the insulating compounds  $(\text{TMTTF})_2\text{X}$ . According to the scaling pictures of § 2.4 and § 2.5, the charge stiffness  $K_\rho = 0$  vanishes in the presence of a gap below  $T_\rho$ , or for  $\ell > \ell_\rho$ . The resulting behavior for the relaxation rate is then

$$T_1^{-1} \sim C_1 + C_0 T \chi_\sigma^2. \quad (63)$$

As shown in Fig. 6, this behavior is indeed found for  $(\text{TMTTF})_2\text{PF}_6$  salt when the relaxation rate data are combined with those of the spin susceptibility ( $T \chi_\sigma^2$ ) in the normal phase above 40 K, namely above the onset of spin-Peierls fluctuations.[81,37] A similar behavior is invariably found in all insulating materials down to low temperature where three-dimensional magnetic or lattice long-range order is stabilized.[22,82,83] Long-range order also prevents the observation of logarithmic corrections in  $C_1$  which are expected to show up in the low temperature limit.

If we now turn our attention to the effect of pressure, the phase diagram of Fig. 4 shows that hydrostatic pressure reduces  $T_\rho$ . At sufficiently high pressure, the insulating behavior merges with the critical behavior associated with the formation of a spin-density-wave state.[84,68,85] The normal phase is then entirely metallic. This change of behavior can also be achieved *via* chemical means. We

have already seen the effect of chemical pressure within the Fabre salts series when for example the monovalent anion Br was put in place of  $\text{PF}_6$  leading to a sizeable decrease of  $T_\rho$  (Fig. 5). When we substitute TMTSF for TMTTF, however, it leads to a larger shift of the pressure scale as exemplified by the normal phase of the Bechgaard salts  $(\text{TMTSF})_2\text{X}$  ( $\text{X}=\text{PF}_6$ ,  $\text{AsF}_6$ ,  $\text{ClO}_4$ , ...), which is metallic. Assuming that there is a temperature domain where a one-dimensional picture applies to mobile carriers, one must have  $K_\rho > 0$ . Therefore the contribution of uniform spin excitations to the relaxation rate becomes more important. For a compound like  $(\text{TMTSF})_2\text{PF}_6$ , which develops a SDW state at  $T_c \approx 12$  K, deviations to the  $T\chi_\sigma^2$  law due to antiferromagnetic correlations become visible below  $T\chi_s^2 \approx 1$  ( $\approx 200$  K); whereas for a ambient pressure superconductor like  $(\text{TMTSF})_2\text{ClO}_4$  ( $T_c \approx 1.2$  K), which is on the right of the  $\text{PF}_6$  salt on the pressure scale, deviations show up at much lower temperature,  $T \approx 30$  K or  $T\chi_s^2 \approx 0.1$  in Fig. 6. Attempts to square these non critical antiferromagnetic enhancements with the Luttinger liquid picture, however, show that  $K_\rho \simeq 0.1$ .[22,38] Figure 6 serves to illustrate how the strength of antiferromagnetic correlations decrease as one moves from the left to the right side of the phase diagram.

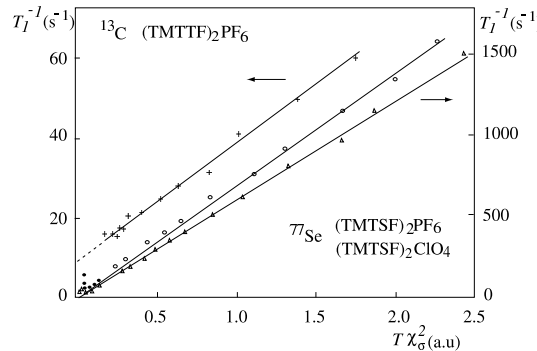


**Fig. 6.** Temperature dependence of the nuclear relaxation rate plotted as  $T_1^{-1}$  vs  $T\chi_\sigma^2(T)$ , where  $\chi_\sigma(T)$  is the measured spin susceptibility.  $(\text{TMTTF})_2\text{PF}_6$  (crosses, left scale),  $(\text{TMTSF})_2\text{PF}_6$  (open circles, right scale) and  $(\text{TMTSF})_2\text{ClO}_4$  (open triangles, right scale). After Ref.[37].

*DC transport and optical conductivity* The metallic resistivity of the Fabre salts ( $T > T_\rho$  in Fig. 5) and of the Bechgaard salts at high temperature has also been analyzed in the one-dimensional framework.[27] It was shown that Umklapp scattering at quarter-filling is the only mechanism of electronic relaxation that can yield metallic resistivity above  $T_\rho$  – half-filling Umklapp alone would lead at small  $K_\rho$  to an insulating behavior at all temperatures.[86] Following Giamarchi [27,87], the prediction at quarter-filling is  $\rho(T) \sim T^{16K_\rho-3}$ , which can reasonably account for the constant volume metallic resistivity observed at high temperature. In the Bechgaard salts for example, an essentially linear tem-

perature dependence  $\rho(T) \sim T^\nu$  with  $\nu \simeq 1$  is found down to 100 K, which would correspond to  $K_\rho \simeq 0.25$  [79,78], a value not too far from NMR estimates for  $(\text{TMTSF})_2\text{PF}_6$ . Below, a stronger power law sets in approaching a Fermi liquid behavior with  $\nu \simeq 2$ , which would indicate the onset of electronic deconfinement. Roughly similar conclusions, as to the value of the charge stiffness  $K_\rho$  and the onset of deconfinement in the Bechgaard salts, have been reached from the analysis of DC transverse resistivity measurements in the high temperature region.[72,88] These are also characterized by a marked change of behavior taking place between 50...100 K.[89]

Optical conductivity measurements on members of both series have recently prompted a lot of interest in the extent to which a one-dimensional description applies to Fabre and Bechgaard salts.[90,70,79,63] As shown in Fig. 7, sulfur compounds show the absence of a Drude weight in the low frequency limit and the infrared conductivity is entirely dominated by an optical gap of the charge sector as expected. It is noteworthy that the optical gap is closer to  $2\Delta_\rho$  than  $\Delta_\rho$ . Following recent work of Essler and Tsvelik, [91] this is consistent with double solitonic excitations in the charge sector and thus a gap produced by quarter-filling Umklapp scattering.

The results for conductivity in the Bechgaard salts came as a surprise, however, since despite the pronounced metallic character of these systems [92], and the existence of a very narrow zero frequency mode, the charge gap still captures most of the spectral weight at high frequencies.[70,79,93] This behavior turns out to mimic that of a doped Mott insulator.[27] According to this picture, the high frequency tail of the conductivity above the gap behave as  $\sigma_1(\omega) \sim \omega^{16K_\rho-5}$  for quarter-filling Umklapp in 1D.[87,94] A power law  $\omega^{-1.3}$  is observed for the Bechgaard salts over more than a decade in frequency (Fig. 7), which yields the value  $K_\rho \simeq 0.23$  for the charge stiffness. This is consistent with the estimate made from DC resistivity. The purely one-dimensional prediction works well in the high frequency range presumably because the effect of interchain hopping is small there ( $\omega > t_{\perp b}$ ). However, deviations from what is expected in a 1D doped Mott insulator are seen at lower frequencies and have been attributed to the influence of  $t_{\perp b}$ .

*Photoemission results* As mentionned earlier in § 2.3, Angular Resolved Photoemission Spectroscopy (ARPES) experiments give in principle access to momentum and energy dependence of the one-particle spectral density  $A(\mathbf{q}, \omega)$  for  $\mathbf{q} < 0$ [95,96]. In practice, this is submitted to the experimental constraints of energy ( $\Delta\omega$ ) and momentum ( $\Delta\mathbf{q}$ ) resolutions, and to thermal broadening. The photoemission signal will then go like [96]

$$I(\mathbf{q}, \omega, T) \sim \sum_{\Delta\omega'} f(\omega') \sum_{\Delta\mathbf{q}'} A(\mathbf{q}', \omega', T),$$

where  $f$  is the Fermi-Dirac distribution. ARPES measurements of Zwick *et al.*,[97] for the Bechgaard salt  $(\text{TMTSF})_2\text{ClO}_4$  and the Fabre salt  $(\text{TMTTF})_2\text{PF}_6$  are shown in Fig. 8. The data are amazing in many respects. In  $(\text{TMTSF})_2\text{ClO}_4$

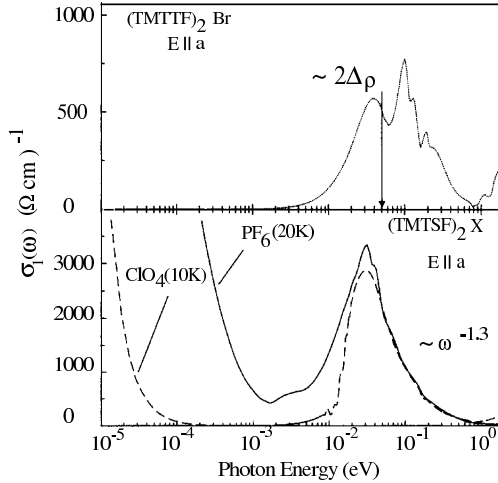


**Fig. 7.** Optical conductivity of the Fabre salt  $(\text{TMTTF})_2\text{Br}$  (top) and the Bechgaard salts  $(\text{TMTSF})_2\text{PF}_6$  and  $(\text{TMTSF})_2\text{ClO}_4$  After Ref. [70].

for example, which is a 1K superconductor (Fig. 4), the data reveal weak spectral intensity at the Fermi level and the absence of dispersing low-energy peaks associated to either spin or charge degrees of freedom. The exponent  $\theta$  needed to describe the ( $\sim$  linear) energy profile of  $I$  down to the non dispersing peak at  $\sim 1$  eV is rather large. Although the origin of these peculiar features is as yet not fully understood, it has been proposed that cleaving and radiation alteration of the surface may introduce imperfections and defects that may change the properties of the Luttinger liquid near the surface.[95,98] Defects can be seen as introducing finite segments of chains with open boundary conditions which correspond to *bounded Luttinger liquids*.[98] Their spectral weight is given by

$$A(\omega) \sim |\omega|^{(2K_\rho)^{-1} - 1/2},$$

which is  $k$ -independent, that is non dispersing but with an exponent that is still governed by the  $K_\rho$  of the bulk. Thus by taking  $K_\rho \simeq 1/3$ , which is actually not too far from the values of other experiments discussed above, would lead to power law compatible with experimental findings.

The ARPES data for the Mott insulating compound  $(\text{TMTTF})_2\text{PF}_6$  reveal similar features apart a clear shift  $\sim 100$  mev of the onset towards negative energy. The shift seems to be close to  $\sim 2\Delta_\rho$ , as expected for quarter-filling Umklapp.[46]

*Dimensionality crossovers and long-range order* Our next task will be to give a brief description of the onset of long-range order in the light of ideas developed earlier in § 3 for an array of weakly coupled 1D electron gas. It was pointed out that the nature of the 1D electronic state strongly influences the way the system undergoes a crossover to a higher dimensional behavior and how this may yield

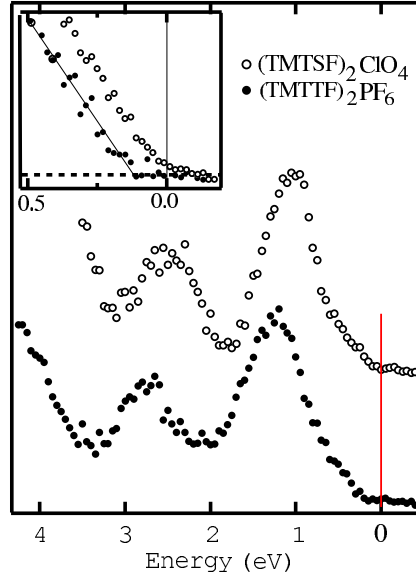


**Fig. 8.** ARPES spectra of  $(\text{TMTTF})_2\text{PF}_6$  and  $(\text{TMTSF})_2\text{ClO}_4$ . The inset identifies an energy shift corresponding to  $2\Delta_\rho$  for  $(\text{TMTTF})_2\text{PF}_6$ . After Ref. [97].

to long-range order. We have seen for example that in the presence of a 1D Mott insulating state, the charge gap gives rise to strong coupling conditions that prevent electronic deconfinement. Spins can still order antiferromagnetically in the transverse direction *via* the interchain exchange  $V_\perp$ . The case of  $(\text{TMTTF})_2\text{Br}$  compound is particularly interesting in this respect since this mechanism can be studied in a relatively narrow pressure interval where the change from strong to weak coupling actually takes place (Fig. 4).

The data of Fig. 9 obtained by Klemme *et al.*, [69] gives the detailed pressure dependence of both  $T_c$  and  $T_\rho$  for the bromine salt up to 13 kbar. When the insulating behavior at  $T_\rho$  meets the critical domain under pressure a maximum of  $T_c$  is clearly seen. This accords well with the description of the transition given in § 3.2 in terms of weakly coupled antiferromagnetic chains (right side of Fig. 3). Here pressure mainly contracts the lattice, modifying upward longitudinal bandwidth while decreasing the stack dimerization. These are consistent with the decrease of correlations along the chains whose strength has been parametrized by  $\theta$  in Fig. 3. Pressure increases  $t_\perp$  too – roughly at the same rate as  $t_\parallel$  [99] – which contributes to the variation of  $\theta$  under pressure.[45] Similar profiles of  $(T_c, T_\rho)$  under pressure have been confirmed in other members of the Fabre salt series. [100,84,101,102]

Passed the maximum, the interchain exchange is gradually replaced by an instability of the Fermi surface to form a SDW state. We have emphasized in § 3.2, however, that this is closely related to the issue of where the onset of electronic deconfinement takes place in the metallic state. In the general phase

diagram of Fig. 4, this fundamental issue applies to the region where the Fabre salt series overlaps with the Bechgaard salt series. In the simple picture given in § 3.1, which is portrayed in Fig. 3, the scale  $T_{x^1}$  for deconfinement and restoration of a Fermi liquid component rises up in the small coupling region. On an empirical basis, however, a clear indication of such a scale is still missing so far and the figures proposed have led to conflicting views. If one agrees for example on the small value of  $K_\rho \simeq 0.2$  given by optics and transport for the Bechgaard salts, the expected  $T_{x^1} \sim 10$  K would be rather small. Although this would be consistent with earlier interpretation of NMR results, [38,22] it contradicts others which favour a Fermi liquid description: the emergence of a  $T^2$  law for parallel resistivity below 100 K, the gradual onset of transverse plasma edge in the same temperature range,[70,103] the  $t_{\perp}$  values extracted from angular dependence of magnetoresistance at very low temperature,[104] the observation of Wiedeman-Franz Law at low temperature,[105] to mention only a few (a more detailed discussion can be found in Refs. [78,79,63]). At present, it is not clear to what extent a synthesis of these conflicting figures will require a radical change of approach in setting out the deconfinement problem or if it simply reflects the fact that deconfinement takes place over a large temperature interval.[45]

Before closing this discussion, we will briefly examine the mechanism commonly held responsible for the suppression of the SDW state as the critical pressure  $P_c$  is approached from below in the phase diagram (Fig. 4). By looking more closely at the effect of pressure on electronic band structure, we realize that corrections to the spectrum such as the longitudinal curvature of the band or transverse hopping  $t_{\perp 2}$  to second nearest-neighbor chains magnify under pressure; their influence can no longer be neglected in the description of the SDW instability of the normal state. In effect, in the presence of an effective  $t_{\perp 2}^*$ , the spectrum below  $T_{x^1}$  becomes

$$E_p(\mathbf{k}) = \epsilon_p(k) - 2t_{\perp}^* \cos k_{\perp} - 2t_{\perp 2}^* \cos 2k_{\perp}.$$

This leads to  $E_+(\mathbf{k} + \mathbf{Q}_0) = -E_-(\mathbf{k}) + 4t_{\perp 2}^* \cos 2k_{\perp}$ , and thus to the alteration of nesting conditions of the whole Fermi surface. These deviations will cut off the infrared singularity of the Peierls channel, which becomes roughly  $\chi^0(\mathbf{Q}_0, T) \sim N(0) \ln(\sqrt{T^2 + \delta^2} / T_{x^1})$ , where  $\delta \sim t_{\perp 2}^*$ . Its substitution in the ladder expression (57) leads to a  $T_c$  that rapidly goes down when  $t_{\perp 2}^* \sim T_c$  (see Fig. 10 for the results of a detailed calculation), in qualitative agreement with experimental findings (Fig. 4).

The strongest support for the relevance of nesting frustration in this part of the phase diagram is provided by the analysis of the cascade of SDW phases at  $P > P_c$ , which are observed when a magnetic field oriented along the less conducting direction is cranked up beyond some threshold.[106,82] In effect, the magnetic field confines the electronic motion in the transverse direction and thus restores the infrared singularity of the Peierls channel at some discrete (quantized) values of the nesting vector, each of which characterizing a SDW phase of the cascade.[107] Besides the indisputable success of a weak coupling (ladder) description of field-induced SDW – which constitutes a whole chapter

of the physics of these materials [108]— some features of the normal phase under field such as the magnetoresistance and NMR refuse to bow to a simple Fermi liquid description. [109]

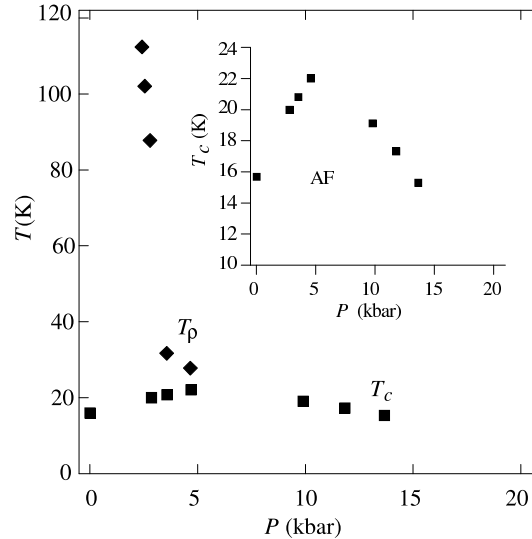


**Fig. 9.** The pressure profile of  $T_p$  (full diamonds) and the antiferromagnetic critical temperature (full squares) for  $(\text{TMTTF})_2\text{Br}$ . After Ref. [69]

*On the nature of superconductivity* Let us now turn our attention to the superconductivity that is found near  $P_c$  for both series, namely at the right hand end of the phase diagram in Fig. 4. The symmetry — singlet or triplet — of the superconducting order parameter in these charge-transfer salts is an open question that is currently much debated<sup>3</sup>.[110,111,112] Here we will tackle this problem from a theoretical standpoint that is in line with what has been previously discussed. We shall give a cursory glance at recent progress made on the origin of organic superconductivity, namely as to whether it could be driven by electronic correlations. In this matter, it is noteworthy that superconductivity shares a common boundary and even overlaps with the SDW state.[85,84,101,65] This close proximity between the two ground states, which is an universal feature of both series of compounds, is peculiar in that it is the electrons of a single band that partake in both types of long-range order. Moreover, SDW correlations are well known to permeate deeply the normal phase above the superconducting phase.[22] All this goes to show that pairings between electrons and holes responsible for antiferromagnetism and superconductivity are not entirely exclusive and that both phenomena may have a common — electronic — origin. [55,52,61,53,54]

<sup>3</sup> See the review of P. M. Chaikin in this volume.

We have become familiar with the mixing of Cooper and Peierls pairings in the context of a Luttinger liquid (see § 2.5). The interference between the two is maximum in strictly one dimension where the Fermi surface reduces to two points. Below the scale  $T_{x^1}$ , interference was neglected in the ladder description of the SDW instability (see § 3.1). However, although interference is weakened by the presence of a coherent wrapping of the Fermi surface, it still exerts an influence below  $T_{x^1}$  by becoming non uniform, that is  $\mathbf{k}$ -dependent along the Fermi surface. As shown recently by Duprat *et al.*,[55] non uniform interference can be taken into account using the renormalization group method of § 2.5. This technique allows us to write down a two-variable flow equation for the SDW coupling constant

$$\begin{aligned} \frac{d\tilde{J}(k_{\perp}, k'_{\perp})}{d\ell} = & - \frac{1}{N_{\perp}} \sum_{k''_{\perp}} \tilde{J}(k_{\perp}, k''_{\perp}) I_C(k''_{\perp}, k'_{\perp}, \ell) \tilde{J}(k''_{\perp}, k'_{\perp}) \\ & + \frac{1}{N_{\perp}} \sum_{k''_{\perp}} \tilde{J}(k_{\perp}, k''_{\perp}) I_P(k''_{\perp}, k'_{\perp}, t_{\perp 2}^*, \ell) \tilde{J}(k''_{\perp}, k'_{\perp}) \end{aligned} \quad (64)$$

where  $I_{C,P}$  are the Cooper loop and the Peierls one in the presence of nesting deviations. The pair of variables  $(k_{\perp}, k'_{\perp})$  refers to transverse momenta of ingoing and outgoing particles that participate in electron-hole and electron-electron pairings close to the Fermi surface.

At small  $t_{\perp 2}^*$ , there is a simple pole singularity in  $J$  at  $k'_{\perp} = k_{\perp} - \pi$ , which signals the expected SDW instability at  $\ell_c = \ln T_c/T_{x^1}$  and wavevector  $\mathbf{Q}_0$  (Fig. 10). As far as  $T_c$  is concerned, this result is qualitatively similar to the ladder approximation of § 3.1. When nesting deviations increase, however,  $T_c$  decreases rapidly and shows an inflection point at a critical  $t_{\perp 2}^{*c}$  instead of reaching zero as for the single channel approximation (Fig. 10). The singular structure of  $J$  in  $k_{\perp}, k'_{\perp}$  space then qualitatively changes, becoming modulated by a product of simple harmonics  $\cos k_{\perp} \cos k'_{\perp}$ . This indicates that singular pairing is now present in the singlet Cooper channel. The attraction takes place between electrons on neighboring stacks as a result of their coupling to spin fluctuations. In the framework of the present model, the singlet superconducting gap  $\Delta(k_{\perp}) = \Delta_0 \cos k_{\perp}$  presents nodes at  $k_{\perp} = \pm\pi/2$ . When typical figures for deviations to perfect nesting are used, that is  $t_{\perp 2,c}^* \sim 10$  K  $\sim T_c(t_{\perp 2}^* \approx 0)$ , the one-loop calculations is able to reproduce an important feature of the phase diagram which is the profiles of SDW and superconductivity in both series of compounds near  $P_c$  (Fig. 4).

## 4.2 The special case of TTF[Ni(dmit)<sub>2</sub>]<sub>2</sub>

Among the very few quasi-one-dimensional organic materials that do not show long-range ordering, the two-chain compound TTF[Ni(dmit)<sub>2</sub>]<sub>2</sub> is interesting.[113,114] The TTF stacks remain metallic down to the lowest temperature reached for this system. Although the reason for this lack of long-range order is not well understood, band calculations revealed a very pronounced quasi-1D anisotropy of the electronic structure,[115] actually stronger than the one of the

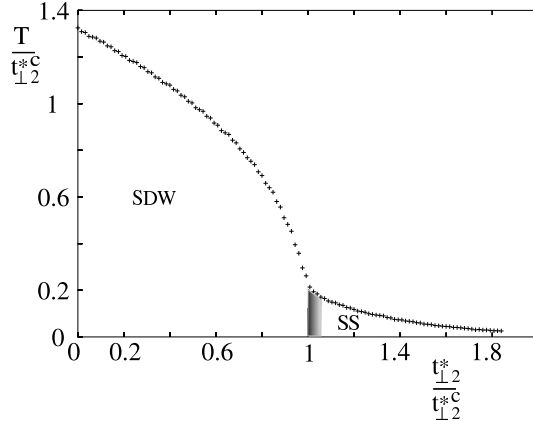


**Fig. 10.** Variation of the critical temperature as a function of nesting deviations  $t_{12}^*$  ( $\sim$  pressure). The shaded area corresponds to the crossover region between SDW and superconductivity. After Ref. [55].

Fabre and the Bechgaard salts. The band filling is not known precisely but it is incommensurate with the underlying lattice. We have here favorable conditions for the emergence of Luttinger liquid physics.

In this respect, the results of Wzietek *et al.*, [114] given in Figure 11 for the temperature variation of the proton ( $^1\text{H}$ ) NMR  $T_1^{-1}$  of the TTF chains, are particularly revealing. When the data of Fig. 11 are compared with the characteristic LL shape of Figure 2 at  $K_\rho > 0$ , the connection with the one-dimensional theory is striking. This is confirmed at the quantitative level by the fit (continuous line in Fig. 11) of data using an expression of the form (48), where the interaction parameter  $K_\rho \simeq 0.3$  have been used. The plot of  $(T_1 T)^{-1}$  *vs*  $T$  (left scale and inset) allows one to isolate the enhancement at low temperature due to the 1D antiferromagnetic response.

### 4.3 An incursion in inorganics: the purple bronze $\text{Li}_{0.9}\text{Mo}_6\text{O}_{17}$

The objective of finding Luttinger liquid behavior in crystals does not focus uniquely on organic conductors but constitutes an important line of research in other materials too. This is the case of molybendum bronzes which form a class of low-dimensional inorganic systems well known for their strongly anisotropic electronic structure and the rich phenomenology associated with the formation of charge-density-wave order.[116] Here we will briefly consider the  $\text{Li}_{0.9}\text{Mo}_6\text{O}_{17}$  compound, which stands out as a special case of the so-called ‘purple bronze’ series. This compound consists of molecular  $\text{MoO}_6$  octahedra and  $\text{MoO}_4$  tetrahedra arranged in a 3D network for which strong Mo-O-Mo interactions form zig-zag chains along a preferential direction. This strong one-dimensional character is confirmed by band calculations [117] and by experimental Fermi surface mapping,[118] which both yield a rather flat Fermi surface arising from the two degenerate bands that cross the Fermi level. The metallic temperature domain

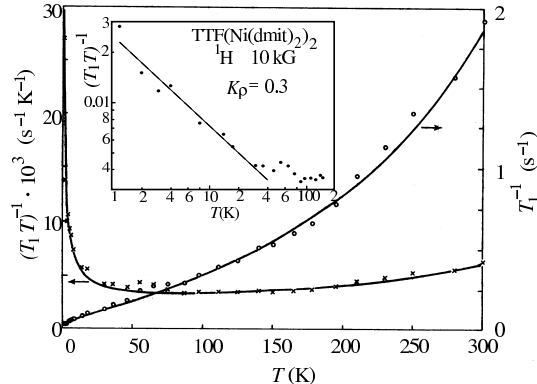


**Fig. 11.** The temperature dependence of the nuclear spin-lattice relaxation rate of TTF[Ni(dmit)<sub>2</sub>]. The continuous line is a Luttinger liquid fit. The power law enhancement at low temperature is shown in the inset. After Wzietek *et al.* [114].

is rather wide, extending down to  $T_c \approx 24$  K where a phase transition occurs. Although the origin of the latter is as yet not well understood, it is not a CDW state and the normal phase does not show any sign of CDW precursors. Therefore electronic interactions dominate and this renders this material particularly appealing for ARPES studies.[118]

Figure 12 shows high resolution ARPES data obtained by Gweon *et al.*, [119] on  $\text{Li}_{0.9}\text{Mo}_6\text{O}_{17}$  at  $T = 250$  K. As one moves along the  $\Gamma - Y$  direction in the Brillouin zone, the lineshape of the C band shifts towards the Fermi edge for increasing  $\mathbf{k} < \mathbf{k}_F$  with a peak that decreases sharply in intensity and broadens significantly before reaching  $\mathbf{k}_F$  to finally pull back for  $\mathbf{k} > \mathbf{k}_F$  and merges in the tail of a weakly dispersing band (B) at high energy. The absence of true crossing of the band, its lack of sharpening as  $\mathbf{k} \rightarrow \mathbf{k}_F$  and the low spectral weight left at  $\mathbf{k}_F$  contrast with what is found in the prototypical Fermi liquid like compound  $\text{TiTe}_2$  [96,120,121]. The analysis of the dispersing lineshape C in the framework of the LL theory proved to be much more satisfactory.[119,96,122,118] A large anomalous exponent  $\theta = 0.9$  and differing values for the velocities  $u_\sigma$  and  $u_\rho$  are required to reasonably account for the data. According to the LL theory of the spectral weight,[13] a large  $\theta$  leads to edges of holon and spinon excitations that crosses the Fermi edge with different amplitudes as shown in Fig. 12-b. The LL theory used in Fig. 13-b is for temperature  $T = 0$  and has  $u_\sigma/u_\rho = 1/5$  as in the analysis of Ref. [118]. Subsequent analysis [122] of the data of Fig. 13-a using a finite temperature theory [15,123] leads to a value of  $u_\sigma/u_\rho = 1/2$ . A large value of  $\theta$  for a system like  $\text{Li}_{0.9}\text{Mo}_6\text{O}_{17}$  with incommensurate band-filling would indicate that long-range Coulomb interactions play an important role in such a system. According to the results of § 3.1, a large  $\theta$  will also yield strong electronic confinement along the chains. The impact on other physical properties should also be observable as for example in the poor conductivity and the absence of a plasma edge in the transverse directions.[124]

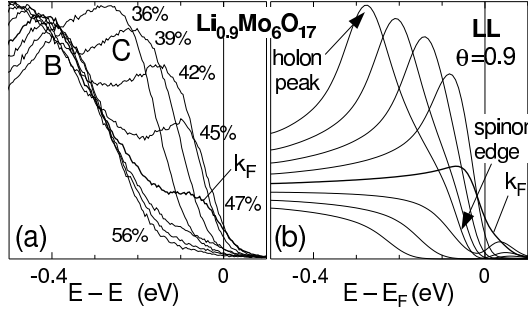


**Fig. 12.** (a) ARPES data at 250 K for  $\text{Li}_{0.9}\text{Mo}_6\text{O}_{17}$  at different % of the Brillouin zone in the  $\Gamma$ -Y direction ; (b) Luttinger liquid prediction at  $\theta = 0.9$ , and  $u_\sigma = u_\rho/5$ , including experimental momentum and energy resolutions, and thermal (Fermi-Dirac) broadening. After Ref. [119].

## 5 Conclusion

A large part of the phenomenology shown by quasi-one-dimensional conductors cannot be understood in the traditional framework of solid state physics. Probably for no other crystals do we have to reckon with concepts provided by the now well understood physics of interacting electrons in one dimension. The existence of long-range order at finite temperature in many of these systems indicates that the link between one and higher-dimensional physics is also essential to their understanding.

As we have seen in this review some progress has been achieved in that direction but there are also several basic questions left to answer. Among them, let us mention how Fermi liquid quasi-particles are appearing in the normal phase for systems like the Bechgaard salts (or their sulfur analogs at high pressure) ? A clarification of this issue would certainly represent a significative advance in the comprehension of these fascinating low-dimensional solids.

**Acknowledgements** The author thanks D. Jérôme, L.G. Caron, R. Duprat, N. Dupuis, J. P. Pouget, A.-M. Tremblay and R. Wortis for numerous discussions on several aspects of this work; J. W. Allen and G.-H. Gweon for several remarks and correspondance about ARPES results on molybdenum bronzes. This work is supported by the Natural Sciences and Engineering Research Council of Canada (NSERC), le Fonds pour la Formation de Chercheurs et l'Aide à la Recherche du Gouvernement du Québec (FCAR), the 'superconductivity program' of the Institut Canadien de Recherches Avancées (CIAR).

## References

1. J. Voit, Rep. Prog. Phys. **58**, 977 (1995).

2. H. J. Schulz, in *Strongly Correlated Electronic Materials: The Los Alamos Symposium 1993*, edited by K. S. Bedell *et al.* (Addison-Wesley, Reading, MA, 1994), p. 187.
3. V. J. Emery, in *Highly Conducting One-Dimensional Solids*, edited by J. T. Devreese, R. E. Evrard, and V. E. van Doren (Plenum Press, New York, 1979), p. 247.
4. J. M. Luttinger, *J. Math. Phys.* **4**, 1154 (1963).
5. D. C. Mattis and E. H. Lieb, *J. Math. Phys.* **6**, 304 (1965).
6. S. Tomonaga, *Prog. Theor. Phys.* **5**, 544 (1950).
7. H. J. Schulz, *J. Phys. C: Solid State Phys.* **16**, 6769 (1983).
8. F. D. M. Haldane, *J. Phys. C* **14**, 2585 (1981).
9. D. C. Mattis, *J. Math. Phys.* **15**, 609 (1974).
10. A. Luther and I. Peschel, *Phys. Rev. B* **9**, 2911 (1974).
11. F. D. M. Haldane, *Phys. Rev. Lett.* **45**, 1358 (1980).
12. J. Voit, *Phys. Rev. B* **47**, 6740 (1993).
13. V. Meden and K. Schonhammer, *Phys. Rev. B* **46**, 15 753 (1992).
14. N. Nakamura and Y. Suzumura, *Prog. Theor. Phys.* **98**, 29 (1997).
15. D. Orgad *et al.*, *Phys. Rev. Lett.* **86**, 4362 (2001).
16. Y. Suzumura, *Prog. Theor. Phys.* **63**, 51 (1980).
17. H. Nélisse *et al.*, *Eur. Phys. J. B* **12**, 351 (1999).
18. W. Metzner and C. D. Castro, *Phys. Rev. B* **47**, 16107 (1993).
19. J. P. Pouget and S. Ravy, *J. Phys. I (France)* **6**, 1501 (1996).
20. J. P. Pouget, in *Physics and Chemistry of Low-Dimensional Inorganic Compounds*, edited by M. G. C. Schlenker, J. Dumas and S. V. Smaalen (Plenum Press, New York, 1996), p. 185.
21. C. Bourbonnais, *J. Phys. I (France)* **3**, 143 (1993).
22. P. Wzietek *et al.*, *J. Phys. I (France)* **3**, 171 (1993).
23. A. Luther and V. J. Emery, *Phys. Rev. Lett.* **33**, 589 (1974).
24. E. Lieb and F. Y. Wu, *Phys. Rev. Lett.* **20**, 1445 (1968).
25. F. Mila and X. Zotos, *Europhys. Lett.* **24**, 133 (1993).
26. S. Barisic and S. Brazovskii, in *Recent Developments in Condensed Matter Physics*, edited by J. T. Devreese (Plenum, New York, 1981), Vol. 1, p. 327.
27. T. Giamarchi, *Physica* **B230-232**, 975 (1997).
28. J. Voit, *Eur. Phys. J. B* **5**, 505 (1998).
29. E. W. Carlson, D. Orgad, S. A. Kivelson, and V. J. Emery, *Phys. Rev. B* **62**, 3422 (2000).
30. Y. A. Bychkov, L. P. Gorkov, and I. Dzyaloshinskii, *Sov. Phys. JETP* **23**, 489 (1966).
31. J. Solyom, *Adv. Phys.* **28**, 201 (1979).
32. C. Bourbonnais and L. G. Caron, *Int. J. Mod. Phys. B* **5**, 1033 (1991).
33. C. Bourbonnais, in *Les Houches, Session LVI (1991), Strongly interacting fermions and high- $T_c$  superconductivity*, edited by B. Doucot and J. Zinn-Justin (Elsevier Science, Amsterdam, 1995), p. 307.
34. C. Bourbonnais, B. Guay, and R. Wortis, in *Theoretical methods for strongly correlated electrons*, edited by A. M. Tremblay, D. Senechal, A. Ruckenstein, and C. Bourbonnais (Springer, Heidelberg, 2002).
35. I. E. Dzyaloshinskii and A. I. Larkin, *Sov. Phys. JETP* **34**, 422 (1972).
36. S. Eggert, I. Affleck, and M. Takahashi, *Phys. Rev. Lett.* **73**, 332 (1994).
37. C. Bourbonnais *et al.*, *Phys. Rev. Lett.* **62**, 1532 (1989).
38. C. Bourbonnais *et al.*, *J. Phys. (Paris) Lett.* **45**, L755 (1984).

39. D. Boies, C. Bourbonnais, and A.-M. Tremblay, Phys. Rev. Lett. **74**, 968 (1995).
40. E. Arrigoni, Phys. Rev. Lett. **80**, 790 (1998).
41. P. W. Anderson, Phys. Rev. Lett. **67**, 3844 (1991).
42. L. G. Caron and C. Bourbonnais, Synthetic Metals **27A**, 67 (1988).
43. H. J. Schulz, Int. J. Mod. Phys. B **5**, 57 (1991).
44. C. Castellani, C. D. Castro, and W. Metzner, Phys. Rev. Lett. **72**, 316 (1994).
45. S. Biermann, A. Georges, A. Lichtenstein, and T. Giamarchi, Phys. Rev. Lett. **87**, 276405 (2001), arXiv:cond-mat/0107633.
46. F. H. L. Essler and A. M. Tsvelik, arXiv:cond-mat/0108382 (unpublished).
47. S. Capponi, D. Poilblanc, and E. Arrigoni, Phys. Rev. B **57**, 6360 (1998).
48. L. Caron and C. Bourbonnais, arXiv:cond-mat/0112071 (unpublished).
49. D. Nelson, Phys. Rev. B **11**, 3504 (1975).
50. V. N. Prigodin and Y. A. Firsov, Sov. Phys. JETP **49**, 369 (1979).
51. W. Kohn and J. M. Luttinger, Phys. Rev. Lett. **15**, 524 (1965).
52. V. J. Emery, Synthetic Metals **13**, 21 (1986).
53. M. T. Béal-Monod, C. Bourbonnais, and V. J. Emery, Phys. Rev. B **34**, 7716 (1986).
54. C. Bourbonnais and L. G. Caron, Europhys. Lett. **5**, 209 (1988).
55. R. Duprat and C. Bourbonnais, Eur. Phys. J. B **21**, 219 (2001).
56. C. Bourbonnais and L. G. Caron, Physica **143B**, 450 (1986).
57. S. Brazovskii and Y. Yakovenko, J. Phys. (Paris) Lett. **46**, L (1985).
58. Y. A. Firsov, Y. N. Prigodin, and C. Seidel, Phys. Rep. **126**, 245 (1985).
59. Strictly speaking, long-range order at finite temperature is impossible in two dimensions for an order parameter with more than one component. However, a finite coupling in the third direction is present which enables to obtain a finite  $T_c$ .
60. V. J. Emery, R. Bruinsma, and S. Barisic, Phys. Rev. Lett. **48**, 1039 (1982).
61. L. G. Caron and C. Bourbonnais, Physica **143B**, 453 (1986).
62. S. Brazovskii and Y. Yakovenko, Sov. Phys. JETP **62**, 1340 (1985).
63. C. Bourbonnais and D. Jérôme, Science **281**, 1156 (1998).
64. C. Coulon *et al.*, J. Phys. (Paris) **43**, 1059 (1982).
65. R. Brusetti, M. Ribault, D. Jérôme, and K. Bechgaard, J. Phys. (Paris) **43**, 801 (1982).
66. J. Pouget *et al.*, Mol. Cryst. Liq. Cryst. **79**, 129 (1982).
67. F. Creuzet, S. P. Parkin, D. Jérôme, and J. Fabre, J. Phys. (Paris) Coll. **44**, 1099 (1983).
68. L. Balicas *et al.*, J. Phys. I (France) **4**, 1539 (1994).
69. B. J. Klemme *et al.*, Phys. Rev. Lett. **75**, 2408 (1995).
70. V. Vescoli *et al.*, Science **281**, 1181 (1998).
71. D. Chow *et al.*, Phys. Rev. Lett. **81**, 3984 (1998).
72. J. Moser *et al.*, Eur. Phys. J. B **1**, 39 (1998).
73. D. S. Chow *et al.*, Phys. Rev. Lett. **85**, 1698 (2000).
74. L. G. Caron, C. Bourbonnais, F. Creuzet, and D. Jérôme, Synthetic Metals **19**, 69 (1987).
75. C. Bourbonnais and B. Dumoulin, J. Phys. I (France) **6**, 1727 (1996).
76. J. Riera and D. Poilblanc, Phys. Rev. B **62**, R16243 (2000), arXiv:cond-mat/0006460.
77. P. Monceau, F. Nad, and S. Brazovskii, Phys. Rev. Lett. **86**, 4080 (2001).
78. C. Bourbonnais and D. Jérôme, in *Advances in Synthetic Metals, Twenty Years of Progress in Science and Technology*, edited by P. Bernier, S. Lefrant, and G. Bidan (Elsevier, New York, 1999), pp. 206–261, arXiv:cond-mat/9903101.

79. A. Schwartz *et al.*, Phys. Rev. B **58**, 1261 (1998).
80. K. Penc and F. Mila, Phys. Rev. B **50**, 11 429 (1994).
81. F. Creuzet *et al.*, Synthetic Metals **19**, 289 (1987).
82. D. Jérôme, in *Organic Conductors: fundamentals and applications*, edited by J.-P. Farges (Dekker, New York, 1994), pp. 405–494.
83. B. Gotschy *et al.*, J. Phys. I (France) **2**, 677 (1992).
84. H. Wilhelm *et al.*, Eur. Phys. J. B **21**, 175 (2001).
85. D. Jérôme, A. Mazaud, M. Ribault, and K. Bechgaard, J. Phys. (Paris) Lett. **41**, L95 (1980).
86. L. P. Gor'kov and I. E. Dzyaloshinskii, JETP Lett. **18**, 401 (1973).
87. T. Giamarchi and A. J. Millis, Phys. Rev. B **46**, 9325 (1992).
88. P. Fertey, M. Poirier, and P. Batail, Eur. Phys. J. B **10**, 305 (1999).
89. J. Moser (unpublished).
90. M. Dressel *et al.*, Phys. Rev. Lett. **77**, 398 (1996).
91. F. H. L. Essler and A. M. Tsvelik, arXiv:cond-mat/0105582 (unpublished).
92. K. Bechgaard *et al.*, Solid State Comm. **33**, 1119 (1980).
93. N. Cao, T. Timusk, and K. Bechgaard, J. Phys. I (France) **6**, 1719 (1996).
94. D. Controzzi, F. H. L. Essler, and A. M. Tsvelik, Phys. Rev. Lett. **86**, 680 (2001).
95. M. Grioni and J. Voit, in *Electron spectroscopies applied to low-dimensional materials*, edited by H. Stanberg and H. Hughes (Kluwer Academic Publ., Netherlands, 2000), p. 501.
96. G.-H. Gweon *et al.*, J. Elec. Spectro. Rel. Phenom. **117-118**, 481 (2001), arXiv:cond-mat/0103470.
97. F. Zwick *et al.*, Phys. Rev. Lett. **79**, 3982 (1997).
98. J. Voit, Y. Wang, and M. Grioni, Phys. Rev. B **61**, 7930 (2000).
99. D. Jérôme and H. Schulz, Adv. in Physics **31**, 299 (1982).
100. D. Jaccard *et al.*, J. Phys.: Condens. Matter **13**, 89 (2001).
101. T. Adachi *et al.*, J. Am. Chem. Soc. **122**, 3238 (2000).
102. P. Auban-Senzier *et al.*, J. Phys. (Paris) **50**, 2727 (1989).
103. C. S. Jacobsen, D. Tanner, and K. Bechgaard, Phys. Rev. Lett. **46**, 1142 (1981).
104. G. M. Danner, W. Kang, and P. M. Chaikin, Phys. Rev. Lett. **72**, 3714 (1994).
105. S. Belin and K. Behnia, Phys. Rev. Lett. **79**, 2125 (1997).
106. P. Chaikin, J. Phys. I (France) **6**, 1875 (1996).
107. L. P. Gorkov and A. G. Lebed, J. Phys. (Paris) Lett. **45**, L433 (1984); M. Hératier, G. Montambaux and P. Lederer, J. Phys. (Paris) Lett. **45**, L943 (1984); K. Yamaji, Synthetic Metals **13**, 19 (1986); L. Chen, K. Maki and V. Virosztek, Physica **143B**, 444 (1986).
108. T. Ishiguro and K. Yamaji, *Organic Superconductors*, Vol. 88 of *Springer-Verlag Series in Solid-State Science* (Springer-Verlag, Berlin, Heidelberg, 1990).
109. K. Behnia *et al.*, Phys. Rev. Lett. **74**, 5272 (1995).
110. I. J. Lee, M. J. Naughton, G. M. Danner, and P. M. Chaikin, Phys. Rev. Lett. **78**, 3555 (1997).
111. I. J. Lee *et al.*, Phys. Rev. Lett. **88**, 17004 (2002).
112. A. G. Lebed, Phys. Rev. B **59**, R721 (1999).
113. L. Brossard *et al.*, C. R. Acad. Sc. Paris **205**, 302 (1986).
114. C. Bourbonnais *et al.*, Europhys. Lett. **6**, 177 (1988).
115. A. Kobayashi *et al.*, Solid State Commun. **62**, 57 (1987).
116. *Physics and Chemistry of Low-Dimensional Inorganic Compounds*, edited by C. Schlenker, J. Dumas, M. Greeblatt, and S. van Smaalen (Plenum Press, New York, 1996).

117. M. H. Whangbo and E. Canadell, *J. Am. Chem. Soc.* **110**, 358 (1988).
118. J. D. Denlinger *et al.*, *Phys. Rev. Lett.* **82**, 2540 (1999).
119. G.-H. Gweon *et al.*, Proc. of Strongly Correlated Electron Systems (SCES), Univ. of Michigan (August 2001), to be published in *Physica B*, arXiv:cond-mat/0107211.
120. T. Straub *et al.*, *Phys. Rev. B* **55**, 13473 (1997).
121. R. Claessen *et al.*, *Phys. Rev. Lett.* **69**, 808 (1992).
122. G.-H. Gweon *et al.* (unpublished).
123. D. Orgad, *Philos. Mag. B* **81**, 375 (2001).
124. L. Degiorgi *et al.*, *Phys. Rev. B* **38**, 5821 (1988).